The transcription factor Foxg1 promotes optic fissure closure in the mouse by suppressing Wnt8b in the nasal optic stalk

JNeurosci
THE JOURNAL OF NEUROSCIENCE

Research Articles: Development/Plasticity/Repair

The transcription factor Foxg1 promotes optic fissure closure in the mouse by suppressing Wnt8b in the nasal optic stalk

Rowena Smith[1], Yu-Ting Huang[1], Tian Tian[1], Dominika Vojtasova[1], Oscar Mesalles-Naranjo[2], Steven M. Pollard[3,4], Thomas Pratt[1], David J. Price[1] and Vassiliki Fotaki[1]

[1]*Edinburgh Medical School: Biomedical Sciences, Centre for Integrative Physiology, Hugh Robson Building, George Square, Edinburgh, EH8 9XD, UK*

[2]*Information Service Division, NHS National Services Scotland, Area 159A, Gyle Square, 1 South Gyle Crescent, Edinburgh, EH12 9EB, UK*

[3]*Medical Research Council (MRC) Centre for Regenerative Medicine, Edinburgh, EH16 4UU, UK*

[4]*Edinburgh Cancer Research UK Cancer Centre, Edinburgh, EH16 4UU, UK*

DOI: 10.1523/JNEUROSCI.0286-17.2017

Received: 30 January 2017

Revised: 25 June 2017

Accepted: 2 July 2017

Published: 20 July 2017

Author contributions: R.S., Y.-T.H., T.T., D.V., and V.F. performed research; R.S., Y.-T.H., T.T., D.V., O.M.-N., T.P., D.J.P., and V.F. analyzed data; O.M.-N. and V.F. designed research; S.M.P. contributed unpublished reagents/analytic tools; T.P., D.J.P., and V.F. wrote the paper.

Conflict of Interest: The authors declare no competing financial interests.

This work was supported by the Medical Research Council [MR/J013137/1]; the Wellcome Trust [085065] and a Medical Research Scotland Vacation Scholarship. We are grateful to the CBS-BRR University of Edinburgh animal house staff for invaluable help with mouse maintenance; J. Mason for the *Wnt8b+/-* mutant mice; the following researchers for sharing plasmids for riboprobe synthesis: A. Goffinet (*Celsr3*, *Fzd3*, *Vangl3*), E. Herrera (*Foxd1*), R. Hindges (*Vax1*), T. Theil (*Bmp7*); the Developmental Studies Hybridoma Bank, University of Iowa (Department of Biological Sciences, Iowa City, IA) for the Islet1 (generated by T. Jessell and S. Brenner-Morton) and Pax6 (generated by A. Kawakami) antibodies; H. Arnheiter for the rabbit polyclonal Mitf antibody; W.K. Chan and V. Allison for technical support during the final phases of the project; A. Kubasik-Thayil for invaluable help with the confocal imaging and the use of the IMARIS software. E. Osterweil's lab for kindly providing access to the StepOnePlus Real-Time PCR machine; M. Molinek for the excellent up-keeping of our communal lab; Z. Kozic for bioinformatics advice and members of our labs for discussions and support.

Corresponding author: Vassiliki Fotaki, Edinburgh Medical School: Biomedical Sciences, Centre for Integrative Physiology, Hugh Robson Building, George Square, Edinburgh, EH8 9XD, UK, vfotaki@ed.ac.uk

Cite as: J. Neurosci ; 10.1523/JNEUROSCI.0286-17.2017

Title Page

Title

The transcription factor Foxg1 promotes optic fissure closure in the mouse by suppressing Wnt8b in the nasal optic stalk

Abbreviated title

Foxg1 suppresses Wnt8b for mouse optic fissure to seal

Authors

Rowena Smith[1,#], Yu-Ting Huang[1&], Tian Tian[1&], Dominika Vojtasova[1&], Oscar Mesalles-Naranjo[2], Steven M. Pollard[3,4], Thomas Pratt[1], David J. Price[1], Vassiliki Fotaki[1]

Affiliations

1: Edinburgh Medical School: Biomedical Sciences, Centre for Integrative Physiology, Hugh Robson Building, George Square, Edinburgh, EH8 9XD, UK

2: Information Service Division, NHS National Services Scotland, Area 159A, Gyle Square, 1 South Gyle Crescent, Edinburgh, EH12 9EB, UK

3: Medical Research Council (MRC) Centre for Regenerative Medicine, Edinburgh, EH16 4UU, UK

4: Edinburgh Cancer Research UK Cancer Centre, Edinburgh, EH16 4UU, UK

#: Present address: MRC Centre for Reproductive Health, Queen's Medical Research Institute, 47 Little France Crescent, Edinburgh, EH16 4TJ, UK

[&]These authors contributed equally to this work

Corresponding author

Vassiliki Fotaki

Edinburgh Medical School: Biomedical Sciences, Centre for Integrative Physiology, Hugh Robson Building, George Square, Edinburgh, EH8 9XD, UK

vfotaki@ed.ac.uk

Number of pages

52

Number of figures

16

Number of tables

4

Number of words – Abstract

250

Number of words – Introduction

646

Number of words – Discussion

1500

Conflict of Interest:

The authors declare no competing financial interests.

Acknowledgements

This work was supported by the Medical Research Council [MR/J013137/1]; the Wellcome Trust [085065] and a Medical Research Scotland Vacation Scholarship. We are grateful to the CBS-BRR University of Edinburgh animal house staff for invaluable help with mouse maintenance; J. Mason for the *Wnt8b+/-* mutant mice; the following researchers for sharing plasmids for riboprobe synthesis: A. Goffinet (*Celsr3*, *Fzd3*, *Vangl3*), E. Herrera (*Foxd1*), R. Hindges (*Vax1*), T. Theil (*Bmp7*); the Developmental Studies Hybridoma Bank, University of Iowa (Department of Biological Sciences, Iowa City, IA) for the Islet1 (generated by T. Jessell and S. Brenner-Morton) and Pax6 (generated by A. Kawakami) antibodies; H. Arnheiter for the rabbit polyclonal Mitf antibody; W.K. Chan and V. Allison for technical support during the final phases of the project; A. Kubasik-Thayil for invaluable

help with the confocal imaging and the use of the IMARIS software. E. Osterweil's lab for kindly providing access to the StepOnePlus Real-Time PCR machine; M. Molinek for the excellent up-keeping of our communal lab; Z. Kozic for bioinformatics advice and members of our labs for discussions and support.

Abstract

During vertebrate eye morphogenesis a transient fissure forms at its inferior part, known as the optic fissure. This will gradually close giving rise to a healthy, spherical optic cup. Failure of the optic fissure to close gives rise to an ocular disorder known as coloboma. During this developmental process *Foxg1* is expressed in the optic neuroepithelium, with highest levels of expression in the nasal optic stalk. *Foxg1-/-* mutant mice have microphthalmic eyes with a large ventral coloboma. We found *Wnt8b* expression upregulated in the *Foxg1-/-* optic stalk and hypothesized that, similar to what is observed in telencephalic development, Foxg1 directs development of the optic neuroepithelium through transcriptional suppression of *Wnt8b*. To test this, we generated *Foxg1-/-;Wnt8b-/-* double mutants of either sex and found that the morphology of the optic cup and stalk and the closure of the optic fissure were substantially rescued in these embryos. This rescue correlates with restored Pax2 expression in the anterior tip of the optic fissure. In addition, although we do not find evidence implicating altered proliferation in the rescue, we observe a significant increase in apoptotic cell density in *Foxg1-/-;Wnt8b-/-* double mutants compared to the *Foxg1-/-* single mutant. Upregulation of Wnt/β-catenin target molecules in the optic cup and stalk may underlie the molecular and morphological defects in the *Foxg1-/-* mutant. Our results show that proper optic fissure closure relies on *Wnt8b* suppression by Foxg1 in the nasal optic stalk to maintain balanced apoptosis and Pax2 expression in the nasal and temporal edges of the fissure.

Significance statement

Coloboma is an ocular disorder that may result in a loss of visual acuity and accounts for around 10% of childhood blindness. It results from errors in the sealing of the optic fissure (OF), a transient structure at the bottom of the eye. Here, we investigate the colobomatous phenotype of the *Foxg1-/-* mutant mouse. We identify upregulated expression of Wnt8b in the optic stalk of *Foxg1-/-* mutants before OF closure initiates. *Foxg1-/-;Wnt8b-/-* double mutants show a substantial rescue of the *Foxg1-/-* coloboma phenotype, which correlates with a rescue in molecular and cellular defects of *Foxg1-/-* mutants. Our results unravel a new role of Foxg1 in promoting OF closure providing additional knowledge about the molecules and cellular mechanisms underlying coloboma formation.

Introduction

Vertebrate eye development is a multi-step process that involves early specification of the eye field followed by bilateral evagination of the diencephalon, giving rise to the optic vesicle. The optic vesicle will then invaginate and form the optic stalk (OS) ventrally and the two-layered optic cup, with an outer layer known as retinal pigment epithelium (RPE) and the inner (close to the lens) neural retina. As the optic cup grows the apposed edges of its inferior part, known as the optic fissure, come in close proximity and fuse together to give rise to a fully formed spherical eye structure (Chow and Lang, 2001; Lamb et al., 2007; Fuhrmann, 2010).

The cellular and molecular mechanisms that control optic fissure closure are not fully understood. Errors underlying this process lead to an ocular disorder known as coloboma. Although environmental factors have been implicated in defective optic fissure closure, it is well established that mutations in genes that are normally expressed in the optic vesicle give rise to coloboma (Gregory-Evans et al., 2004; Chang et al., 2006; Williamson and FitzPatrick, 2014).

The study of animal models with colobomatous phenotypes has allowed a better understanding regarding the cellular and molecular basis of the disorder. Among the cellular processes underlying optic cup formation and optic fissure closure are cell proliferation and apoptotic cell death.

Among the molecules that are involved in coloboma formation is the transcription factor Pax2. Mutations in the *PAX2* gene in humans lead to the renal-coloboma syndrome characterized by renal and ocular malformations, including optic nerve coloboma (Schimmenti et al., 1995; Schimmenti, 2011). Loss of Pax2 in mice leads to a coloboma phenotype due to inability of the edges of the optic fissure to fuse (Torres et al., 1996). New molecular players are continuously added to the list of genes leading to coloboma in mice and humans (Gregory-Evans et al., 2004; Chang et al., 2006; Williamson and FitzPatrick, 2014), including proteins implicated in the HH (Wen et al., 2015), Fgf (Cai et al., 2013), Bmp (Huang et al., 2015), RA (Lupo et al., 2011) and Wnt (Liu and Nathans, 2008; Zhou et al., 2008; Lieven and Ruther, 2011; Liu et al., 2012; Alldredge and Fuhrmann, 2016; Liu et al., 2016) signalling pathways.

106 *Foxg1* is forkhead box transcription factor expressed from early stages of mouse embryonic
107 development in the developing nervous system and is specifically found in the telencephalon, optic
108 chiasm and retina (Xuan et al., 1995; Huh et al., 1999; Pratt et al., 2004; Fotaki et al., 2006; Tian et
109 al., 2008; Fotaki et al., 2013). Mice with no functional Foxg1 (*Foxg1-/-* mutants) die at birth and show
110 severe reduction in the size of telencephalic lobes and eyes (Xuan et al., 1995). In addition, *Foxg1-/-*
111 eyes display a large ventral coloboma (Huh et al., 1999). Foxg1's role in the developing eye has not
112 been studied in detail. We have recently shown that in the mouse Foxg1 is essential for controlling the
113 size of the ciliary margin in the nasal peripheral retina and for suppressing Wnt/β-catenin signalling in
114 this region (Fotaki et al., 2013).

115 Here, we examine the molecular and cellular causes of the coloboma phenotype of the *Foxg1-/-*
116 mutant. We found that *Wnt8b* expression in the wild type OS is upregulated in this mutant. We
117 hypothesized that, similar to the telencephalon (Danesin et al., 2009), Foxg1 may normally suppress
118 *Wnt8b* in the nasal OS for proper optic cup and/or OS formation to take place. We tested this by
119 suppressing Wnt8b expression genetically in *Foxg1-/-;Wnt8b-/-* double mutants. In accordance with
120 our hypothesis, in the double mutant we found substantial rescue of the optic fissure closure defect we
121 observed in the *Foxg1-/-* single mutant. Our results reveal a novel mechanism of optic fissure closure
122 which relies on Foxg1-mediated suppression of *Wnt8b* in the nasal OS to maintain balanced apoptosis
123 and normal Pax2 expression in the nasal edges of the fissure.

Materials and methods

Mice

All experiments were done according to Home Office regulations (Scotland, UK).

Foxg1+/- heterozygote males were bred to F1 (CBAxC57/B6) females to produce *Foxg1*+/- heterozygous males and females as previously described (Fotaki et al., 2013). The *Wnt8b*+/- mice have been previously described (Fotaki et al., 2010). *Foxg1*+/-;*Wnt8b*+/- double heterozygotes were generated by intercrossing *Foxg1*+/- and *Wnt8b*+/- heterozygous mice.

Embryos

To generate *Foxg1*-/- single or *Foxg1*-/-;*Wnt8b*-/- double mutant embryos, timed matings were set up among *Foxg1*+/- heterozygote or *Foxg1*+/-;*Wnt8b*+/- double heterozygote male and female mice respectively. The day the vaginal plug was detected in females was designated as E0.5.

No gross differences were detected in morphology or marker expression between wild types (*Foxg1*+/+) and Foxg1+/- heterozygotes (not shown). However, unless otherwise stated, in most cases when comparing *Foxg1*-/- homozygotes to controls we used wild type embryos.

Foxg1-/-;*Wnt8b*-/- double mutant embryos were compared to two experimental groups: a) a control group, consisting of either wild type (*Foxg1*+/+;*Wnt8b*+/+), single heterozygotes (*Foxg1*+/-;*Wnt8b*+/+ *or* *Foxg1*+/+;*Wnt8b*+/-) or double heterozygote (*Foxg1*+/-;*Wnt8b*+/-) embryos; b) a group where the *Foxg1* mutation was found in homozygosis (*Foxg1*-/-) and the *Wnt8b* allele was either wild type (*Wnt8b*+/+) or heterozygous (*Wnt8b*+/-). This group was collectively named as the *Foxg1*-/-;*Wnt8b*+/± mutant group.

Genotyping of mice and embryos

Foxg1+/- heterozygote mice express one copy of functional β-galactosidase under the control of the Foxg1 promoter and were distinguished from wild types (*Foxg1*+/+) by PCR analysis based on detection of the lacZ allele (Xuan et al., 1995). For all embryos younger than E11.0, the *Foxg1* mutation was detected by PCR using primers specific for the *Foxg1*-wild type allele (Foxg1-wt-F:

AGG CTG ACG CAC TTG GAG; Foxg1-wt-R: CAG GGG TTG AGG GAG TAG GT), resulting in a 856 bp PCR product and for the *Foxg1*-null allele (Foxg1-mt-F: GCT GGA CAT GGG AGA TAG GA; Foxg1-mt-R: GAC AGT ATC GGC CTC AGG AA), resulting in a 650 bp PCR product. For embryos older than E11.0, *Foxg1-/-* mutants were clearly distinguished by their phenotype as previously described (Fotaki et al., 2013).

The *Wnt8b* mutation was detected by PCR in both mouse and embryonic tissue as previously described (Fotaki et al., 2010).

Histology and cresyl violet staining

Mouse embryos were collected on ice-cold PBS buffer and fixed in 4% paraformaldehyde (PFA) in 0.1M Phosphate buffer as previously described (Fotaki et al., 2006). Embryos were either embedded in a 1:1 mixture of OCT/sucrose (30%) for cryostat sectioning or in paraffin for microtome sectioning (Fotaki et al., 2013). Embryos used for cell counts were embedded in paraffin and cut at 7 μm horizontal sections. Some sections were stained with 0.2% of cresyl violet acetate (Sigma-Aldrich, Dorset, UK).

Riboprobe synthesis, in situ hybridization (ISH), immunohistochemistry, immunofluorescence, X-gal staining

Probes were labeled with digoxigenin according to the manufacturer's instructions (Roche, Burgess Hill, UK). Riboprobes used for this study were for *Axin2* (Fotaki et al., 2011), *Bmp7* (Morcillo et al., 2006), *Celsr3* (Tissir et al., 2005), *Foxg1* (Fotaki et al., 2013), *Foxd1* (Herrera et al., 2004), *Fzd3* (Montcouquiol et al., 2006), *Vangl* (Montcouquiol et al., 2006), *Vax1* (Bertuzzi et al., 1999), *Wnt2b* (Fotaki et al., 2013), *Wnt3a*, *Wnt5a* (Liu et al., 2003; Ang et al., 2004) and *Wnt7b*, *Wnt8b* (as described in Fotaki et al., 2011).

Previously described protocols were used for in situ hybridization, immunohistochemistry, immunofluorescence and X-gal staining (Fotaki et al., 2008, 2011; Fotaki et al., 2013). Pax2 DAB-immunohistochemistry was performed on already X-gal stained sections of *Foxg1+/-* embryos (Figure 11 - panels A&B). DAB-immunohistochemistry for β-gal was performed on sections that had already

been reacted for *Wnt8b* ISH (Figure 3). Following incubation with the appropriate secondary biotylinated antibody, DAB-immunohistochemistry was performed using the Vectastain ABC kit (Vector, Peterborough, UK), as previously described (Fotaki et al., 2006). ISH sections were in many cases counterstained with Nuclear Fast Red (Vector). Immunofluorescence reacted sections were counterstained with 4′,6-Diamidine-2′-phenylindole dihydrochloride (DAPI) dilactate (2 μg/ml) (Sigma-Aldrich). All experiments were performed on at least 6 eyes from 3 different embryos for each experimental group (unless otherwise indicated).

All antibodies used for experiments are listed in Table 1. All Alexa-fluorescent antibodies were from Molecular Probes - ThermoFischer Scientific (Loughborough, UK).

Imaging

DAB and in situ images were taken with a Leica DFC480 camera connected to a Leica DMNB epifluorescence microscope. Fluorescence images were taken with a Leica DM5500B automated upright microscope connected to a DFC360FX camera. Whole embryonic eyes were photographed with a Leica DFC420 camera connected to a Leica M165C stereomicroscope all from Leica Microsystems (Milton Keynes, UK). Confocal images were taken with a Zeiss LSM 510 Axioskop.

Labelling Index (LI), Mitotic Index, Apoptotic Cell Density and Pax2 Cell Density Counts

To calculate the LI we used *Foxg1*+/+ wild type controls (n= 4 eyes from 3 different embryos) and *Foxg1*-/- mutants (n= 5 eyes from 3 different embryos). Using confocal images, we counted the total number of cells counterstained with DAPI and the total number of cells immunostained with BrdU from 3-4 dorsal to ventral sections from the nasal and temporal components of the retina. Cell counts were performed manually on merged stacks of confocal images using the software IMARIS 8.0.0 (Bitplane, RRID:SCR_007370), which allows image rotation, facilitating counts in the x-y-z axis. LI was calculated as the ratio of BrdU-positive to the total number of cells in the nasal and temporal retinae.

To calculate the pHH3 cell surface density (mitotic index) we used *Foxg1*+/+ wild type controls (n= 4 eyes from 3 different embryos) and *Foxg1*-/- mutants (n= 5 eyes from 3 different embryos). The

total number of pHH3-positive cells was counted manually in the nasal and temporal retinae of each section from 3-4 dorsal to ventral sections. ImageJ (RRID:SCR_003070) was used to outline and calculate the perimeter of the apical surface of the nasal and temporal retinae, where counts were taken from and the volume of each section was calculated by multiplying the thickness of the section (7 μm) by the area.

To calculate the apoptotic cell density in our first experimental setup (Table 2) we used *Foxg1+/+* wild type controls (n= 5 eyes from 3 different embryos) and *Foxg1-/-* mutants (n= 5 eyes from 3 different embryos) and in our second experimental setup (Table 3) we used control (n= 6 eyes from 4 different embryos), *Foxg1-/-;Wnt8b+/±* (n= 4 eyes from 2 different embryos) and *Foxg1-/-;Wnt8b-/-* double mutant (n= 4 eyes from 3 different embryos) embryos. We counted cleaved caspase-3 positive cells from 3-5 middle to ventral sections from each eye where optic fissure was detectable and omitted dorsal sections, as cell death detection in these was absent from all our experimental groups. The area of the nasal and temporal retinae, where counts were taken from, was traced using ImageJ and the volume of each section was calculated by multiplying the thickness of the section (7 μm) by the area.

To calculate the Pax2 cell density at the edges of the optic fissure, we used control (n= 3 eyes from 3 different embryos); *Foxg1-/-;Wnt8b+/±* mutant (n= 4 eyes from 3 different embryos) and *Foxg1-/-;Wnt8b-/-* double mutant (n= 3 eyes from 3 different embryos) embryos. We counted Pax2-positive cells from 2 representative mid-sagittal sections within a square of 0.1 mm x 0.1 mm encompassing the edges of the fissure and the average values for the nasal and temporal retinae of each specimen were used for comparisons.

Corrected Total Cell Fluorescence (CTCF) counts

To quantitate Pax6 and Pax2 expression we used controls (for E10.5: n= 5 eyes & for E11.5: n= 4 eyes from 3 different embryos); *Foxg1-/-;Wnt8b+/±* mutants (for E10.5: n= 6 eyes & E11.5: n= 4 eyes from 3 different embryos) and *Foxg1-/-;Wnt8b-/-* double mutants (for E10.5 & E11.5: n= 4 eyes from 3 different embryos) at E10.5 and E11.5. Using ImageJ, we outlined the nasal and temporal retinae and for each section we measured the area, the mean fluorescence and the integrated

fluorescent density, along with several adjacent background readings in 3-6 representative sections per specimen along the ventro-dorsal axis. The most dorsal sections were not included in the study as their morphological differences in the mutants are more subtle than those observed in middle and ventral sections. For each section we calculated the CTCF according to the formula: CTCF = Integrated Density – (Selected Area X Mean fluorescence of background readings) (McCloy et al., 2014). The obtained values were divided by 1000.

Statistics

To compare the LI, mitotic index and apoptotic cell density between our different experimental groups, we assumed that this follows a normal distribution within the mouse population of the same genotype and that two values were different when the confidence intervals did not intersect. The confidence intervals were calculated using the mean values (LI, mitotic index or apoptotic cell density), the standard error and the value of the normal distribution that corresponds to at least 95% confidence level ($p \leq 0.05$), after applying the Bonferroni correction where appropriate. For our calculations, we used a sampling strategy. We used a two-stage sampling strategy (Shiver and Borders, 1996), in which the primary units are the mouse eyes and the secondary units are the eye sections. This sampling strategy, a widely used methodology in experimental fields such as Forestry, is applied, for example, to calculate total number of trees and/or ratios among specific species (Shiver and Borders, 1996).

Data analysis was performed using R software (version 3.1.2, RRID:SCR_001905) and the package survey for analysis of complex surveys (http://r-survey.r-forge.r-project.org/survey/). The package survey produces an estimate of the mean ratio (LI=Brdu-positive cells/Total number of cells; cell density=cell count/volume) and its standard error (SE).

To compare the Pax6 and Pax2 CTCF values we performed ANOVA analysis followed by Bonferroni correction, using the averaged CTCF values along the ventro-dorsal axis for the nasal and temporal retina of each specimen analysed. A similar procedure was followed to calculate the Pax2-positive cell density in the nasal and temporal retinae. The degrees of freedom (df), the F value and the p value were calculated using the software SPSS (IBM SPSS Statistics 21, RRID:SCR_002865).

RNA extraction, cDNA synthesis and PCR-arrays

The optic cups of E11.0 wild type and *Foxg1-/-* age-matched embryos were dissected out using fine tip (0.125 mm) Tungsten dissecting probes (WPI, Hitchin, UK) and snap frozen on dry ice. RNA was generated pooling together 6 eyes, dissected out from 3-5 different wild type or *Foxg1-/-* mutant embryos and was extracted using the RNeasy micro kit (QIAGEN, Manchester, UK) following the manufacturer's instructions. 150 ng of RNA from three independent samples of *Foxg1+/+* wild type and *Foxg1-/-* mutant optic cups were used to synthesize cDNA, using the RT2 First Strand Kit (QIAGEN) according to the manufacturer's instructions. The cDNA was mixed with RT2 SYBR Green ROX qPCR mastermix (QIAGEN) according to the manufacturer's instruction and the mixture was loaded on RT2 Profile PCR array plates for the mouse Wnt signalling pathway [PAMM-043Z] (QIAGEN). The plates were run on a StepOnePlus Real-Time PCR machine (Applied Biosystems, ThermoFisher Scientific). Results obtained from three plates for each group were further processed through the QIAGEN GeneGlobe Data Analysis Centre (http://www.qiagen.com/gb/shop/genes-and-pathways/data-analysis-center-overview-page/).

Results

Expression of *Foxg1* in the developing optic cup and stalk at E10.5

Foxg1 expression in the developing mouse retina has been described in detail at E12.5 and E14.5, after completion of optic fissure closure (Huh et al., 1999; Pratt et al., 2004; Tian et al., 2008; Fotaki et al., 2013). To gain understanding about *Foxg1* expression in the developing optic cup before the optic fissure seals, we performed in situ hybridization at E10.5 on horizontal sections throughout the ventral-to-dorsal axis (Figure 1). *Foxg1* expression was detected in the nasal retina and RPE (optic cup) and in the OS in agreement with previous observations (Hatini et al., 1994). *Foxg1* expression was higher in ventral and middle sections compared to dorsal sections (compare Figure 1a-c to 1d). In ventral sections, *Foxg1* expression appeared more extended towards the midline of the naso-temporal axis than in middle and dorsal sections and reached the nasal edge of the optic fissure (arrow in Figure 1a). *Foxg1* expression in the optic cup was lower than that in the OS and telencephalon throughout the ventral-to-dorsal axis (i.e. compare intensity of telencephalic and OS to optic cup signal in Figure 1A-C). Our results highlight high expression of Foxg1 in the nasal optic stalk and ventral optic cup, both of which are involved in optic fissure formation.

Increased *Wnt8b* expression in the *Foxg1-/-* optic stalk at E10.5

In the mouse telencephalon, Foxg1 suppresses expression of Wnt molecules (*Wnt2b*, *Wnt3a*, *Wnt5a*, *Wnt7b* and *Wnt8b*), normally confined to the dorsomedial telencephalon and/or cortical hem (not shown & Muzio and Mallamaci, 2005; Hanashima et al., 2007). We hypothesized that the same Wnt molecules are also upregulated in the developing optic vesicle leading to defects in optic fissure closure. Using in situ hybridization, we examined expression of these Wnts in wild type E12.0-E12.5 horizontal sections to determine expression in the optic cup and stalk.

All five Wnt molecules examined were expressed in the dorsomedial telencephalon and/or cortical hem (Figure 2A,C,E,G,I), as previously described (Richardson et al., 1999; Muzio and Mallamaci, 2005; Fotaki et al., 2010 & data not shown). In the optic neuroepithelium, *Wnt8b* was detected in a small domain in the OS (Figure 2B, arrowhead in 2b) (Roy et al., 2013). *Wnt7b*-positive cells were

observed in the lens (Figure 2D,d) (Liu et al., 2003; Ang et al., 2004), while *Wnt2b* expression was confined in the peripheral RPE and ciliary margin (Figure 2F,f) (Liu et al., 2003; Fotaki et al., 2013). *Wnt5a* was detected in the eyelid epithelium (Figure 2H,h), as previously reported (Liu et al., 2003; Kumar and Duester, 2010), while *Wnt3a* was not detected in any part of the developing optic cup or stalk or surrounding periocular mesenchyme (Figure 2J,j) (Liu et al., 2003).

We then studied expression of *Wnt2b*, *Wnt7b* and *Wnt8b* which were found expressed in the optic neuroepithelium, in E10.5 horizontal sections of control and *Foxg1-/-* mutants by means of in situ hybridization. No differences were observed in *Wnt2b* and *Wnt7b* expression in the E10.5 optic cup between wild types and *Foxg1-/-* mutants (not shown). Similar to E12.5, at E10.5 *Wnt8b* expression in the wild type developing optic vesicle was restricted to a small domain in the OS (Figure 3A,a). However in the *Foxg1-/-* mutant, *Wnt8b* expression at and near the OS region was found expanded (Figure 3A', arrowheads in Figure 3a'). In controls, *Wnt8b* expression was found in both the nasal and temporal OS and nasally it was expressed in Foxg1-positive cells (reflected by positive β-gal staining, expressed under the control of the Foxg1 promoter, Figure 3B,b). In *Foxg1-/-* mutants, *Wnt8b* expansion was observed in the nasal optic stalk, where Foxg1 is normally expressed (Figure 3B',b').

Our results indicate that loss of Foxg1 leads to an upregulation of *Wnt8b* in the developing nasal OS, in a domain where Foxg1 is normally expressed, suggesting that Foxg1 may normally suppress Wnt8b function in this region.

Significant rescue of the coloboma phenotype of the *Foxg1-/-* mutant in a *Wnt8b*-null genetic background

Based on expansion of *Wnt8b* expression in the *Foxg1-/-* OS at E10.5 (Figure 3) and the previously described repressor activity of foxg1 on wnt8b in the zebrafish telencephalon (Danesin et al., 2009), we hypothesized that upregulated Wnt8b expression in the optic stalk causes coloboma in the *Foxg1-/-* mutant. To test our hypothesis, we crossed male and female mice, double heterozygous for the *Foxg1* (*Foxg1+/-*) (Xuan et al., 1995) and *Wnt8b* (*Wnt8b+/-*) (Fotaki et al., 2010) alleles, to generate double homozygous embryos *Foxg1-/-;Wnt8b-/-*.

We first assessed the phenotype of *Wnt8b-/-* mutant optic cups at E15.5. Cresyl violet staining showed similar optic cup morphology between wild type and *Wnt8b-/-* mutants and complete closure of the optic fissure (Figure 4A,A'). In addition, double immunofluorescence for markers of the proliferating (BrDU and Vsx2) and differentiating (Tuj1 and Islet1) retinal layers did not reveal any gross differences between wild types and *Wnt8b-/-* mutants (Figure 4B,B' & 4C,C').

We then examined the eye phenotype of control, *Foxg1-/-;Wnt8b+/+* or *Foxg1-/-;Wnt8b+/-* (collectively designated as *Foxg1-/-;Wnt8b+/±* mutants) and *Foxg1-/-;Wnt8b-/-* double mutants at E15.5, when optic fissure closure has normally been completed. Control eyes showed normal optic cup morphology and complete optic fissure closure (Figure 5A). *Foxg1-/-;Wnt8b+/±* mutants displayed microphthalmia and ventral coloboma (Figure 5A'), as previously described (Huh et al., 1999). As predicted by our hypothesis, *Foxg1-/-;Wnt8b-/-* double mutants displayed a spherical-shaped optic cup and rescue of the coloboma phenotype (Figure 5A'').

Gross analysis of optic cup morphology did not reveal a large ventral gap in any of the *Foxg1-/-;Wnt8b-/-* double mutant eyes examined (n=12). Cresyl violet staining showed a spherical optic cup and optic nerve in control embryos (Figure 5B), an abnormal optic cup with an elongated retina with foldings and with no clearly identifiable optic nerve in *Foxg1-/-;Wnt8b+/+* mutants (100% of all eyes examined; n= 22) (Figure 5B') (Pratt et al., 2004) and an optic cup and optic nerve resembling that of controls in *Foxg1-/-;Wnt8b-/-* double mutants (Figure 5B''). Sequential coronal sections of *Foxg1-/-;Wnt8b-/-* double mutant eyes (n=6) revealed that 50% of the optic cups had complete optic fissure closure anteriorly and at the mid-lenticular level and 100% at the posterior pole (Figure 5C'-E'). At anterior and mid-lenticular levels, 50% of the optic cups showed unfused tips in the form of small gaps or indentations (Figure 5C',D'),which were never observed in controls (n=18 eyes) (Figure 5C,D). The indentations anteriorly included both the interior and exterior aspects of the *Foxg1-/-;Wnt8b-/-* neural retina (arrowheads in Figure 5C'), while at mid-lenticular level it either included both (not shown) or just the interior aspect (arrowhead in Figure 5D'). The edges of the optic fissure of the *Foxg1-/-;Wnt8b-/-* optic cup at the posterior pole were fused and resembled those of controls (Figure 5E,E').

Our results collectively show a spectacular rescue of the optic cup and optic stalk/nerve morphology and of the optic fissure closure defect observed in the *Foxg1-/-* mutant in a genetic background lacking *Wnt8b* expression and strongly suggest that *Wnt8b* expression normally needs to be suppressed by Foxg1 for normal optic cup and stalk development to take place.

Naso-temporal defects are not rescued in the *Foxg1-/-;Wnt8b-/-* double mutant retina

Foxg1 is crucial for specification of the nasal retina and its loss leads to an abnormal expansion of the temporal expression of Foxd1 nasally (Huh et al., 1999; Tian et al., 2008). We hypothesized that the rescue of the double mutant *Foxg1-/-;Wnt8b-/-* optic cup morphology (Figure 5B''), may be the result of a rescue in naso-temporal retinal patterning. In situ hybridization for *Foxd1* expression at E11.5 and E15.5 revealed restricted expression in the temporal retina in controls (Figure 6A,B) and expanded expression in the nasal domain of *Foxg1-/-;Wnt8b+/±* retinae (Figure 6A',B'). In the *Foxg1-/-;Wnt8b-/-* double mutant we observed a similar expansion of *Foxd1* to that observed in the *Foxg1-/-;Wnt8b+/±* retinae at E11.5 and E15.5 (Figure 6A''& 6B''). Results were similar at E10.5 and consistent for all specimens analysed (8 eyes from 4 different embryos for each experimental group, across all ages), indicating that rescued morphology of the optic cup in *Foxg1-/-;Wnt8b-/-* double mutants occurs despite the retention of naso-temporal patterning defects.

The *Foxg1-/-;Wnt8b-/-* double mutant optic cup morphology at E10.5 resembles that of the *Foxg1-/-* single mutant

To understand when in development we first start to observe morphological differences between controls, *Foxg1-/-;Wnt8b+/±* mutants and *Foxg1-/-;Wnt8b-/-* double mutants, we examined the morphology and marker expression of the optic neuroepithelium in these experimental groups at E10.5. Using as markers Coup-TFI, which labels the retina and the OS (Tang et al., 2010), and Mitf, which labels the RPE (Nguyen and Arnheiter, 2000), we first observed major morphological differences between wild types and *Foxg1-/-* single mutants along the naso-temporal axis (Figure 7). Coup-TFI expression was detected throughout the ventral optic cup (Figure 7A,A'), while in dorsal sections it showed a ^{high}temporal-^{low}nasal gradient (Figure 7D,D & Tang et al., 2010) in wild types and *Foxg1-/-* mutants. Coup-TFI expression revealed that in ventral sections the *Foxg1-/-* optic cup

displayed an abnormal flattened shape (Figure 7A') compared to the wild type U-shaped optic cup (Figure 7A). In addition, the forming optic fissure in wild types (asterisk in Figure 7C) was not detectable in the Foxg1-/- mutant (question mark in Figure 7C'). Coup-TFI expression in the OS, although similar between wild types and *Foxg1-/-* mutants, revealed an abnormally enlarged distance between nasal and temporal OS in the *Foxg1-/-* mutant (double arrow in Figure 7C'). Regarding Mitf expression, this was limited to the RPE in wild types and *Foxg1-/-* mutants (Figure 7B,B',E,E'), but revealed a thickened nasal RPE in the *Foxg1-/-* mutant in both ventral (Figure 7B') and dorsal (Figure 7E') sections.

We then examined our three experimental groups described above using well-established markers for the retina, RPE, and OS [Pax6: in the retina with ^{high}peripheral-to-^{low}central gradient and a ^{low}ventral-to-^{high}dorsal gradient & in the RPE (Walther and Gruss, 1991; Baumer et al., 2003)]; [Coup-TFII: in the RPE & OS – (Tang et al., 2010; Eiraku et al., 2011)]; [Pax2: in the OS and central retina with a ^{high}ventral-to-^{low}dorsal gradient (Nornes et al., 1990; Puschel et al., 1992; Baumer et al., 2003)] to determine differences in optic neuroepithelium morphology and marker expression. Results described below were consistent for all specimens from the same experimental group (6 eyes from 3 different embryos for each experimental group).

In terms of morphology, the ventral optic cup of the *Foxg1-/-;Wnt8b-/-* double mutant was similar to that of the *Foxg1-/-;Wnt8b+/+* mutant, showing a flattened appearance and lack of the U-shape formation in controls due to lack of nasal invagination of the optic cup (arrows in Figure 8A'',C'' and 8A',C'). However in dorsal sections, *Foxg1-/-;Wnt8b-/-* double mutant optic cups resembled the control optic cup shape (Figure 8B,B''&8D,D''). To determine whether the changes in *Foxg1-/-* optic cup morphology may be attributed to defects in the formation of the "hinge" region at the nasal RPE-retinal transition, we examined expression of the phosphorylated myosin light chain 2 (pMLC2), which has been implicated in RPE stiffness and in shaping the optic cup (Eiraku et al., 2011; Carpenter et al., 2015). However, we did not observe any gross differences in pMLC2 expression between E10.5 wild type and *Foxg1-/-* mutant optic cups at the hinge region that may account for the changes observed in the mutant nasal optic cup shape (Figure 7G,G').

In terms of molecular profile, our marker analysis revealed that in the *Foxg1-/-;Wnt8b+/+* single mutant, the Pax2-positive domain seemed reduced in the nasal retina in ventral sections compared to that of controls (compare areas indicated by magenta brackets in Figures 8A,C & 8A',C'), while Pax6 expression seemed expanded nasally in both ventral and dorsal sections compared to that of controls (compare areas indicated by green brackets in Figures 8C & 8C' and Figure 8D to 8D'). However in *Foxg1-/-;Wnt8b-/-* double mutants, Pax2 expression ventrally expanded throughout the nasal and temporal retinal domain (magenta bracketed area in Figure 8A''), similar to that of controls, while Pax6 staining was restricted to the peripheral retina both nasally and temporally and resembled more that of control staining (green bracketed area in Figure 8C'' & Figure 8D'').

To quantitate the above observations, we measured the corrected total cell fluorescence (CTCF) for the Pax6 and Pax2 cells in the nasal and temporal retinae (for details see Materials and Methods). The Pax6 CTCF was found increased in the *Foxg1-/-;Wnt8b+/+* single mutant compared to that of controls and *Foxg1-/-;Wnt8b-/-* double mutants (ANOVA; df, 2; F, 4.433, p=0.036) and the difference reached statistical significance between single and double mutants (Figure 8E,F). In the case of Pax2, although the CTCF was found reduced in the *Foxg1-/-;Wnt8b+/+* single mutant compared to that of controls and double mutants, the difference was not significant (ANOVA; df, 2; F, 0.5; p=0.619) (Figure 8E).

Our results show that at E10.5, ventral optic cup morphology in the *Foxg1-/-;Wnt8b-/-* double mutant resembles more that of *Foxg1-/-;Wnt8b+/+* single mutants than that of controls, despite the fact that Pax6 expression in significantly reduced in these mutants compared to that of the *Foxg1-/-;Wnt8b+/+* single mutant.

Morphological and molecular alterations in optic fissure development in *Foxg1-/-* embryos are rescued in *Foxg1-/-;Wnt8b-/-* double mutants by E11.5

We then examined the morphology and marker expression of the developing optic cup at E11.5, using the same markers as for E10.5 embryos (Coup-TFII/Pax2 and Pax6/Pax2) (Figure 9). As for the E10.5 embryos, results described below were consistent for all specimens from the same experimental group (6 eyes from 3 different embryos for each experimental group).

At E11.5, optic cup morphology in *Foxg1-/-;Wnt8b+/±* mutants was severely compromised in ventral and middle sections (Figure 9A',B',D',E') while the appearance of dorsal optic cup sections resembled more that of controls (Figure 9C,C'& 9F,F'). Coup-TFII expression revealed a thickened RPE in ventro-nasal sections in this mutant (Figure 9A'). The gap between the nasal and temporal edges of the optic fissure was much greater in *Foxg1-/-;Wnt8b+/±* mutants compared to controls (compare the OF region indicated by an arrow in Figures 9A & 9A') and Pax2 expression along the adjoining sides was reduced temporally and was absent nasally (Figure 9A',D'). Similar to controls (Figure 9D-F), Pax6 expression in *Foxg1-/-;Wnt8b+/±* mutants was detected in the retina and RPE (Figure 9D'-F'). However, in ventral sections Pax6 expression revealed a greater nasal domain compared to the Pax6-positive temporal domain (compare the bracketed nasal and temporal retinae in Figure 9D').

In contrast, in *Foxg1-/-;Wnt8b-/-* double mutants the anatomy of the optic cup resembled that of controls along the ventro-dorsal axis (Figure 9A''-F''). In ventral sections, the optic cup displayed a clearly centrally-placed optic fissure between the juxtaposed nasal and temporal sides (Figure 9A'',D''). Although the distance between the edges of the optic fissure in the *Foxg1-/-;Wnt8b-/-* double mutant was not as narrow as that of controls, it was greatly reduced compared to that of the *Foxg1-/-;Wnt8b+/±* mutant (compare the OF region indicated by an arrow in Figures 9A'' to that in 9A & 9A'). The Coup-TFII staining revealed a normal RPE appearance ventro-nasally and not the thickening observed in *Foxg1-/-;Wnt8b+/±* mutants (Figure 9A''). In ventral sections, Pax2 expression in the optic cup was increased compared to *Foxg1-/-;Wnt8b+/±* mutants and surrounded both the nasal and temporal edges of the *Foxg1-/-;Wnt8b-/-* optic fissure (Figure 9A'',D''). Similar to controls, Pax6 expression was detected in the optic cup and RPE (Figure 9D''-F'').

Similar to E10.5, we quantitated expression of Pax6 and Pax2 using the corrected total cell fluorescence along the ventro-dorsal axis. In agreement with our observations, we found a significant increase in Pax6 fluorescence (ANOVA; df, 2; F, 17.29; $p=0.001$) (Figure 10A,C) and a significant decrease in Pax2 fluorescence (ANOVA; df, 2; F, 23.665; $p<0.0001$) (Figure 10B,C) in *Foxg1-/-*

455 *;Wnt8b+/±* mutants compared to that of controls and double mutants. In addition, Pax2 fluorescence
456 was significantly increased in double mutants compared to that of controls (Figure 10B,C).

457 The above results show an amelioration of optic cup and optic stalk morphology in the *Foxg1-/-*
458 *;Wnt8b-/-* double mutant by E11.5, with wild type levels of optic cup Pax6 expression and a
459 significant increase in nasal optic cup Pax2 expression compared to that of wild types and *Foxg1-/-*
460 *;Wnt8b+/±* mutants.

461 To validate rescue of Pax2 expression in the edges of the *Foxg1-/-;Wnt8b-/-* optic fissure, we further
462 examined sagittal sections immunostained for Pax2. First, we examined Pax2 expression in *Foxg1-/-*
463 single mutants and wild type littermates at E12.0, when optic fissure closure is initiated in controls
464 (Figure 11). In contrast to wild type expression (Figure 11A-C), in *Foxg1-/-* retinae the anterior tip
465 was Pax2-negative and located at a distance from the Pax2-positive-posterior optic fissure tip (Figure
466 11C'). Similar results were obtained with in situ hybridization for *Vax1* (Figure 11D,D',E,E'), which
467 is also expressed at the edges of the optic fissure (Baumer et al., 2002) and, when mutated, gives rise
468 to a coloboma phenotype in mice (Hallonet et al., 1999). However, similar expression of *Bmp7*, a
469 gene essential for optic fissure formation (Morcillo et al., 2006), was observed in both the anterior and
470 posterior tips of wild types and *Foxg1-/-* mutants along the proximo-distal axis (Figure 11F,F',G,G').

471 In *Foxg1-/-;Wnt8b-/-* E11.5 sagittal sections (4 eyes from 3 different embryos in the sagittal plane),
472 Pax2 expression was present in both the anterior and posterior tips of the *Foxg1-/-;Wnt8b-/-* optic
473 fissure (Figure 12A'') along the proximo-distal axis (3/4 eyes examined), similar to controls (Figure
474 12A). In one case, anterior Pax2 staining in distal sections was limited to only a few cells (not shown).
475 However, in the *Foxg1-/-;Wnt8b+/±* mutant, Pax2 expression was not detected in the anterior optic
476 fissure (Figure 12A'), in agreement with the results we observed in the *Foxg1-/-* single mutant (Figure
477 11C,C'). This was further confirmed by counting the Pax2-positive cells at the edges of the optic
478 fissure within a square area of 0.01 mm^2 (for details see Materials and Methods). The Pax2-positive
479 cell density in the nasal edge of the optic fissure was significantly reduced in the *Foxg1-/-;Wnt8b+/±*
480 mutant compared to that of controls and double mutants (ANOVA; df, 2; F, 141,374; $p<0.0001$)

(Figure 12B). No differences were observed in temporal Pax2-positive cell density between groups (ANOVA; df, 2; F, 3,669; p=0.081).

These results confirm that loss of Wnt8b function in the *Foxg1-/-* null background leads to a specific increase in Pax2 expression in the anterior (nasal) tips of the optic fissure, strongly suggesting that this may contribute to the rescue of the coloboma phenotype in the *Foxg1-/-;Wnt8b-/-* double mutant.

Cell proliferation is not altered in the *Foxg1-/-* mutant at E10.5

Optic cup formation and optic fissure closure rely on balanced cell proliferation and cell death (Morcillo et al., 2006; See and Clagett-Dame, 2009; Cai et al., 2013; Noh et al., 2016).

To understand whether aberrant optic cup cell proliferation may be involved in coloboma formation in the *Foxg1-/-* mutant, we calculated the labelling index (LI) (BrDU-positive cells over total number of cells) in nasal and temporal retinae of E10.5 wild type and *Foxg1-/-* mutant optic cups (for a detailed description see Materials and Methods)**.** To define the border between nasal and temporal retina, we used as a guide *Foxg1+/-* heterozygous and *Foxg1-/-* homozygous sections immunostained for β-galactosidase (β-gal) (Xuan et al., 1995), normally found in the nasal retina (dashed line in Figure 13A,A'). Our cell counts did not reveal any significant differences in the LI $\pm$ standard error among wild type (0.45170 $\pm$ 0.05608) and *Foxg1-/-* mutant (0.45398 $\pm$ 0.03902) nasal retina or wild type (0.42959 $\pm$ 0.03825) and *Foxg1-/-* mutant (0.43340 $\pm$ 0.05842) temporal retina. In addition, immunohistochemistry for phosphorylated histone H3 (pHH3), a mitosis (M)-phase marker (Hans and Dimitrov, 2001), did not result in any differences in the cell distribution or the mitotic index (number of pHH3-positive cells per surface area $\pm$ standard error) (for details see Materials and Methods) between E10.5 wild type (0.03483 $\pm$ 0.00454) and *Foxg1-/-* mutant (0.03418 $\pm$ 0.00266) nasal retina or wild type (0.03133 $\pm$ 0.00337) and *Foxg1-/-* mutant (0.03686 $\pm$ 0.00772) temporal retina. Finally, based on the suggestion that precocious differentiation of neural progenitors at the apposed edges of the optic fissure may result in failure of the fissure to seal (Lohnes et al., 1994), we performed immunohistochemistry for β-tubulin III (Tuj1), a marker of early-born neurons (Memberg and Hall,

1995). However, we did not observe any Tuj1-positive cells in the E10.5 developing optic cup or OS of wild types or *Foxg1-/-* mutants (not shown).

Apoptotic defects in the nasal retina in the *Foxg1-/-* mutant at E10.5 are partially rescued in the *Foxg1-/-;Wnt8b-/-* double mutant

To determine if abnormal apoptosis is associated with the optic cup phenotype of *Foxg1-/-* mutants, we examined the apoptotic density in E10.5 nasal and temporal wild type and *Foxg1-/-* horizontal sections, using immunohistochemistry for cleaved caspase-3 (Noh et al., 2016). Our cell counts revealed a significantly lower density of apoptotic cells ($p<0.05$) in the *Foxg1-/-* nasal retina compared to that of wild types (Figure 13 & Table 2), with a mean value reaching 35pp (percentage points) of the wild type nasal values. No differences in apoptotic density were observed among genotypes in the temporal retina (Figure 13 & Table 2).

The correlation between decreased nasal apoptosis and failed optic fissure closure in *Foxg1-/-* mutants led us to hypothesise that the rescue of optic fissure closure in the *Foxg1-/-;Wnt8b-/-* double mutant observed at E11.5 (Figure 9A'',D''), is associated with restoration of normal apoptotic levels. We analysed apoptotic cell density in three experimental groups: i. controls; ii. *Foxg1-/-;Wnt8b+/+* mutants and iii. *Foxg1-/-;Wnt8b-/-* double mutants. In nasal retina, and in accordance with our hypothesis, we found an increase of 24pp in mean apoptotic density in *Foxg1-/-;Wnt8b-/-* double mutants compared to *Foxg1-/-;Wnt8b+/+* mutants, which was statistically significant ($p<0.05$) (Figure 14 & Table 3), although the increase did not quite reach the level observed in our control samples ($p<0.05$) (Figure 14 & Table 3). No significant differences were observed in temporal apoptotic cell density between controls, *Foxg1-/-;Wnt8b+/+* mutants and *Foxg1-/-;Wnt8b-/-* double mutants (Table 3).

Our results show that at E10.5 there is significant increase in nasal apoptotic cell density in the *Foxg1-/-;Wnt8b-/-* double mutant compared to the *Foxg1-/-;Wnt8b+/+* mutant, consistent with the idea that this may be partly responsible for the amelioration of the *Foxg1-/-;Wnt8b-/-* optic fissure morphology at E11.5.

Upregulation of Wnt/β-catenin signalling target molecules in the *Foxg1-/-* optic cup and stalk

Wnt molecules signal mainly through the Wnt/β-catenin or the planar cell polarity (PCP) pathways (reviewed in Loh et al., 2016). To gain insight into which Wnt signalling pathway is affected by the upregulation of *Wnt8b* observed in the optic stalk of the *Foxg1-/-* mutant, we examined downstream targets of the Wnt/β-catenin and the PCP pathways in the optic cup and OS.

First, we performed a PCR array analysis and profiled the expression of 84 genes related to Wnt-mediated signal transduction, using RNA extracted from optic cups of E11.0 wild type and *Foxg1-/-* embryos. Out of 12 Wnt-signalling target genes included in the array (indicated by an asterisk in Table 4), the only one that showed a significant change in expression was c-Jun, a downstream target of the Wnt/β-catenin pathway (Mann et al., 1999), with a 2.5-fold upregulation (p=0.01) in *Foxg1-/-* optic cups (Table 4). This upregulation became apparent at the protein level by E12.0, when we detected a clear increase in c-Jun expression in the *Foxg1-/-* retina (Figure 15A,A') (results were consistent in n=6 from 3 different control and *Foxg1-/-* mutant eyes).

We then analysed mRNA expression by means of in situ hybridization in the OS of wild type and *Foxg1-/-* mutants of molecules implicated in the PCP pathway (*Fzd3*, *Celsr3* and *Vangl3*) (Figure 15B-D, B'-D') (Tissir et al., 2005; Montcouquiol et al., 2006), as well as *Axin2* (Figure 15E,E'), a read-out of the Wnt/β-catenin signalling pathway (Jho et al., 2002). *Axin2* showed a clear upregulation in the OS of the *Foxg1-/-* mutant (Figure 15E'), similar to the upregulation observed in *Wnt8b* expression (Figure 15F,F'), which became evident as early as E10.5 (data not shown).

These results show that Wn8b upregulation in the *Foxg1-/-* optic stalk results in upregulation of the Wnt/β-catenin signalling pathway through overexpression of the downstream targets *c-Jun* and *Axin2* in the *Foxg1-/-* mutant optic cup and stalk respectively.

554 **Discussion**

555 Our data unravel a novel mechanism of optic fissure (OF) closure which relies on Foxg1-mediated
556 suppression of *Wnt8b* in the nasal OS resulting in balanced apoptosis and normal Pax2 expression in
557 the nasal edges of the fissure (Figure 16A-C). This newly described role of Foxg1 in optic cup
558 formation is independent of its function as a retinal naso-temporal determinant.

559 We hypothesized that, similar to foxg1 function in the zebrafish telencephalon (Danesin et al., 2009),
560 mouse Foxg1 suppresses Wnt8b function in the developing optic neuroepithelium for proper optic cup
561 formation to take place. Indeed, wild type *Wnt8b* expression in the OS was upregulated in the *Foxg1-*
562 */-* mutant as early as E10.5. This was observed in the nasal stalk, which is the region of the developing
563 optic neuroepithelium with highest *Foxg1* expression levels at this developmental stage (this study
564 and Hatini et al., 1994). Our genetic experiment allowed us to evaluate the in vivo effects of loss of
565 Wnt8b expression in a *Foxg1*-null genetic background. The remarkable rescue of the optic cup and
566 stalk morphology and the substantial sealing of the OF by E15.5 in the *Foxg1-/-;Wnt8b-/-* mutant are
567 in agreement with our hypothesis. Future experiments will show whether mouse retinal Foxg1
568 suppresses Wnt8b by direct binding, similar to zebrafish telencephalon (Danesin et al., 2009), or
569 whether the suppression is indirect, supported by the lack of Foxg1 binding sites within the Wnt8b
570 promoter region in mouse neural stem cells (Bulstrode et al., 2017).

571 Foxg1 is expressed in the nasal retina of vertebrates (Hatini et al., 1994; Takahashi et al., 2003; Picker
572 et al., 2009) and work in chick and zebrafish has established Foxg1's role as an early determinant of
573 retinal naso-temporal polarity exerting an antagonistic effect on Foxd1 (Yuasa et al., 1996; Takahashi
574 et al., 2003), a temporal retina determinant which is abnormally expressed in the *Foxg1-/-* nasal retina
575 (Huh et al., 1999; Tian et al., 2008). The fact that abnormal Foxd1 expression in the nasal retina is
576 still observed in the *Foxg1-/-;Wnt8b-/-* mutant reveals that the coloboma phenotype is not a secondary
577 defect to the abnormal *Foxg1-/-* naso-temporal patterning.

578 Although the shape of the *Foxg1-/-;Wnt8b-/-* optic cup resembles that of the *Foxg1-/-* mutant at
579 E10.5, its Pax6 and Pax2 expression profiles mimic those of controls. By E11.5, the *Foxg1-/-;Wnt8b-*

/- optic cup morphology resembles that of controls, with normal Pax6 and elevated Pax2 expression levels. The optic cup normally undergoes a series of morphological changes, from a flattened to a spherical shape (Lamb et al., 2007; Eiraku et al., 2011; Eiraku and Sasai, 2012). Our data support the idea that in the *Foxg1-/-;Wnt8b-/-* mutant, optic cup formation is delayed resulting in closure of the OF at a later developmental point, at ~E15.5 rather than at E13.5 (Hero, 1989).

Pax2 is required for OF closure (Torres et al., 1996) and loss of Pax2 expression in the nasal (anterior) edge of the optic fissure in the *Foxg1-/-* mutant may account for failure of the OF edges to fuse. This is further supported by the fact that in the *Foxg1-/-;Wnt8b-/-* mutant with 100% OF fusion in proximal sections there is 100% rescue of Pax2 expression in the anterior OF proximally, while in distal sections, where Pax2 expression is not fully recovered, we observe less efficient rescue (Figure 16A-C).

Precise regulation of cellular events is crucial for the development of the optic cup and stalk. At early stages of optic cup development intense cell proliferation takes place, which is associated with the invagination of the optic vesicle and the appearance of the OF (Calvente et al., 1988). We hypothesized that changes in optic cup morphology in the *Foxg1-/-* mutant may result from aberrant proliferation, which may be rescued in the *Foxg1-/-;Wnt8b-/-* mutant. However, the lack of difference in the LI, mitotic index and β-tubulin-III expression between wild types and *Foxg1-/-* mutants at E10.5 argued against the idea that aberrant proliferation and/or premature differentiation is involved in the early *Foxg1-/-* optic cup morphological defects.

Programmed cell death (apoptosis) in the nasal and temporal edges adjoining the OF normally occurs during mouse optic cup formation and OF closure (Hero, 1989; Ozeki et al., 2000). Apoptosis is first detected in ventro-nasal retina in the region of the presumptive OF at E9.5 and is then found in the OF edges, becoming undetectable after the edges fuse at E13.5 (Ozeki et al., 2000). In addition, either increased or decreased OF apoptosis has been found in mouse mutants with a coloboma phenotype (Cai et al., 2013; Noh et al., 2016). This evidence strongly supports balanced apoptosis at the edges of the OF as a major determinant of proper OF closure. Our data show significantly reduced levels of caspase-3 mediated apoptosis in the *Foxg1-/-* ventro-nasal retina, which strongly suggest a

requirement for Foxg1 in promoting apoptotic cell death at the nasal edge of the fissure. Reduction in apoptosis is observed in *Bmp7-/-* mouse mutants, which fail to form OF (Morcillo et al., 2006). However, normal *Bmp7* expression in the edges of the *Foxg1-/-* fissure indicates that Foxg1 OF function is independent of Bmp7. In the *Foxg1-/-;Wnt8b-/-* double mutant, apoptosis in the nasal retina was significantly higher to that of *Foxg1-/-;Wnt8b+/+* mutants, suggesting that Wnt8b overexpression is a contributing factor to the reduction in apoptosis we observe in the *Foxg1-/-* embryos.

Wnt8b activates Wnt/β-catenin signalling (Lee et al., 2006) and our data suggest that upregulation of this signalling cascade results in coloboma. Although our present data do not provide a direct link between the observed changes in apoptosis and Wnt/β-catenin signalling, it is interesting that the only downstream target with upregulated expression in the *Foxg1-/-* optic cup was *c-Jun*. c-Jun protects cells from excessive apoptotic activity (Wisdom et al., 1999; Shaulian and Karin, 2002) and its upregulation in the *Foxg1-/-* mutant optic cup may result in reduction of apoptosis in the nasal edge of the optic fissure compromising fissure closure.

Although our array analysis in the optic cup did not reveal differences between wild types and *Foxg1-/-* mutants in *Axin2* expression, a read-out of the Wnt/β-catenin pathway (Jho et al., 2002), *Axin2* was found upregulated in the *Foxg1-/-* OS, at the same sites where *Wnt8b* upregulation was observed. This is in agreement with the current notion that Wnt proteins are locally-acting signalling molecules (Alexandre et al., 2014; Farin et al., 2016; Loh et al., 2016) and suggests that the rescued optic cup morphology in the *Foxg1-/-;Wnt8b-/-* mutant may be a secondary effect to a primary rescue in OS formation. This idea is further supported with the following model of molecular interactions in the developing eye at ~E11.5 (Figure 16D-F).

Foxg1 in the nasal ciliary margin controls Wnt2b levels, which in turn result in normal transcriptional activation of Pax6. In parallel, Foxg1 in the nasal stalk keeps Wnt8b levels in check, resulting in normal Pax2 expression in the ventral retina, due to low transcriptional repression. Finally, Pax6 and Pax2 levels are balanced through reciprocal inhibition, as previously described (Schwarz et al., 2000)(Figure 16D). When Foxg1 function is abolished, Pax6 expression is upregulated resulting in an

634 expanded ciliary margin (Fotaki et al., 2013), while Pax2 expression is significantly reduced (this
635 study) resulting in failure of the OF to form properly (Figure 16E). In the *Foxg1-/-;Wnt8b-/-* mutant,
636 Pax2 levels are significantly increased compared to those of single mutants and controls (this study),
637 resulting in proper OF closure. Although Pax6 expression should still be elevated in the double
638 mutant, our quantitation analysis reveals similar levels of expression to those of controls. A possible
639 explanation for this is that in the double mutant Pax2 expression is more elevated than that of Pax6,
640 and when it suppresses Pax6 it reduces it to normal values (Figure 16F). Although currently
641 unavailable, we predict that a *Pax2*-overexpressing mouse strain crossed to the *Foxg1*-mutant
642 background will phenocopy the *Foxg1-/-;Wnt8b-/-* phenotype in line with our hypothesis.

643 Our observations that upregulated Wnt/β-catenin signalling associate with coloboma formation seem
644 to be at odds with the fact that a coloboma phenotype is also observed in cases when the Wnt/β-
645 catenin signalling is reduced, as in the case of humans with mutations in the Wnt receptor gene *FZD5*
646 (Liu et al., 2016) and *Fzd5-/-* null mice, which show increased apoptosis and increased Pax2
647 expression in the optic cup (Liu and Nathans, 2008). However, Wnt/β-catenin signalling must also be
648 increased in *Dkk1+/-* mice with reduced levels of the Wnt antagonist Dkk1 and in mice with a loss of
649 function of Axin2, a negative regulator of the Wnt/β-catenin signalling, both of which also show a
650 coloboma phenotype (Lieven and Ruther, 2011; Alldredge and Fuhrmann, 2016). This all suggests
651 that Wnt/β-catenin signalling needs to be tightly regulated in the optic cup and stalk for proper optic
652 fissure closure and unbalanced expression (over- or under-expression) of its components leads to
653 coloboma.

654 Our work uncovers a novel action of Foxg1 in limiting Wnt/β-catenin signalling in the optic stalk for
655 proper optic cup and stalk formation and OF closure to take place and provides additional knowledge
656 regarding the molecular players and cellular mechanisms underlying coloboma formation.

References

Alexandre C, Baena-Lopez A, Vincent JP (2014) Patterning and growth control by membrane-tethered Wingless. Nature 505:180-185.

Alldredge A, Fuhrmann S (2016) Loss of Axin2 Causes Ocular Defects During Mouse Eye Development. Invest Ophthalmol Vis Sci 57:5253-5262.

Ang SJ, Stump RJ, Lovicu FJ, McAvoy JW (2004) Spatial and temporal expression of Wnt and Dickkopf genes during murine lens development. Gene Expr Patterns 4:289-295.

Baumer N, Marquardt T, Stoykova A, Ashery-Padan R, Chowdhury K, Gruss P (2002) Pax6 is required for establishing naso-temporal and dorsal characteristics of the optic vesicle. Development 129:4535-4545.

Baumer N, Marquardt T, Stoykova A, Spieler D, Treichel D, Ashery-Padan R, Gruss P (2003) Retinal pigmented epithelium determination requires the redundant activities of Pax2 and Pax6. Development 130:2903-2915.

Bertuzzi S, Hindges R, Mui SH, O'Leary DD, Lemke G (1999) The homeodomain protein vax1 is required for axon guidance and major tract formation in the developing forebrain. Genes Dev 13:3092-3105.

Bulstrode H, Johnstone E, Marques-Torrejon MA, Ferguson KM, Bressan RB, Blin C, Grant V, Gogolok S, Gangoso E, Gagrica S, Ender C, Fotaki V, Sproul D, Bertone P, Pollard SM (2017) Elevated FOXG1 and SOX2 in glioblastoma enforces neural stem cell identity through transcriptional control of cell cycle and epigenetic regulators. Genes Dev 31:757-773.

Burns CJ, Zhang J, Brown EC, Van Bibber AM, Van Es J, Clevers H, Ishikawa TO, Taketo MM, Vetter ML, Fuhrmann S (2008) Investigation of Frizzled-5 during embryonic neural development in mouse. Dev Dyn 237:1614-1626.

680 Cai Z, Feng GS, Zhang X (2010) Temporal requirement of the protein tyrosine phosphatase Shp2 in
681 establishing the neuronal fate in early retinal development. J Neurosci 30:4110-4119.

682 Cai Z, Tao C, Li H, Ladher R, Gotoh N, Feng GS, Wang F, Zhang X (2013) Deficient FGF signaling causes
683 optic nerve dysgenesis and ocular coloboma. Development 140:2711-2723.

684 Calvente R, Carmona R, Abadia-Molina F, Abadia-Fenoll F (1988) Stereological study on the mode of
685 optic cup expansion and the accumulation of mitoses in the early stages of chick embryo
686 development. Anat Rec 222:401-407.

687 Carpenter AC, Smith AN, Wagner H, Cohen-Tayar Y, Rao S, Wallace V, Ashery-Padan R, Lang RA
688 (2015) Wnt ligands from the embryonic surface ectoderm regulate 'bimetallic strip' optic cup
689 morphogenesis in mouse. Development 142:972-982.

690 Chang L, Blain D, Bertuzzi S, Brooks BP (2006) Uveal coloboma: clinical and basic science update. Curr
691 Opin Ophthalmol 17:447-470.

692 Chow RL, Lang RA (2001) Early eye development in vertebrates. Annu Rev Cell Dev Biol 17:255-296.

693 Danesin C, Peres JN, Johansson M, Snowden V, Cording A, Papalopulu N, Houart C (2009) Integration
694 of telencephalic Wnt and hedgehog signaling center activities by Foxg1. Dev Cell 16:576-587.

695 Eiraku M, Sasai Y (2012) Self-formation of layered neural structures in three-dimensional culture of
696 ES cells. Curr Opin Neurobiol 22:768-777.

697 Eiraku M, Takata N, Ishibashi H, Kawada M, Sakakura E, Okuda S, Sekiguchi K, Adachi T, Sasai Y
698 (2011) Self-organizing optic-cup morphogenesis in three-dimensional culture. Nature 472:51-56.

699 Farin HF, Jordens I, Mosa MH, Basak O, Korving J, Tauriello DV, de Punder K, Angers S, Peters PJ,
700 Maurice MM, Clevers H (2016) Visualization of a short-range Wnt gradient in the intestinal stem-cell
701 niche. Nature 530:340-343.

Fotaki V, Yu T, Zaki PA, Mason JO, Price DJ (2006) Abnormal positioning of diencephalic cell types in neocortical tissue in the dorsal telencephalon of mice lacking functional Gli3. J Neurosci 26:9282-9292.

Fotaki V, Price DJ, Mason JO (2008) Newly identified patterns of Pax2 expression in the developing mouse forebrain. BMC Dev Biol 8:79.

Fotaki V, Larralde O, Zeng S, McLaughlin D, Nichols J, Price DJ, Theil T, Mason JO (2010) Loss of Wnt8b has no overt effect on hippocampus development but leads to altered Wnt gene expression levels in dorsomedial telencephalon. Dev Dyn 239:284-296.

Fotaki V, Price DJ, Mason JO (2011) Wnt/beta-catenin signaling is disrupted in the extra-toes (Gli3(Xt/Xt)) mutant from early stages of forebrain development, concomitant with anterior neural plate patterning defects. J Comp Neurol 519:1640-1657.

Fotaki V, Smith R, Pratt T, Price DJ (2013) Foxg1 is required to limit the formation of ciliary margin tissue and Wnt/beta-catenin signalling in the developing nasal retina of the mouse. Dev Biol 380:299-313.

Fuhrmann S (2010) Eye morphogenesis and patterning of the optic vesicle. Curr Top Dev Biol 93:61-84.

Gregory-Evans CY, Williams MJ, Halford S, Gregory-Evans K (2004) Ocular coloboma: a reassessment in the age of molecular neuroscience. J Med Genet 41:881-891.

Hallonet M, Hollemann T, Pieler T, Gruss P (1999) Vax1, a novel homeobox-containing gene, directs development of the basal forebrain and visual system. Genes Dev 13:3106-3114.

Hanashima C, Fernandes M, Hebert JM, Fishell G (2007) The role of Foxg1 and dorsal midline signaling in the generation of Cajal-Retzius subtypes. J Neurosci 27:11103-11111.

Hans F, Dimitrov S (2001) Histone H3 phosphorylation and cell division. Oncogene 20:3021-3027.

725 Hatini V, Tao W, Lai E (1994) Expression of winged helix genes, BF-1 and BF-2, define adjacent
726 domains within the developing forebrain and retina. J Neurobiol 25:1293-1309.

727 Hero I (1989) The optic fissure in the normal and microphthalmic mouse. Exp Eye Res 49:229-239.

728 Herrera E, Marcus R, Li S, Williams SE, Erskine L, Lai E, Mason C (2004) Foxd1 is required for proper
729 formation of the optic chiasm. Development 131:5727-5739.

730 Huang J, Liu Y, Oltean A, Beebe DC (2015) Bmp4 from the optic vesicle specifies murine retina
731 formation. Dev Biol 402:119-126.

732 Huh S, Hatini V, Marcus RC, Li SC, Lai E (1999) Dorsal-ventral patterning defects in the eye of BF-1-
733 deficient mice associated with a restricted loss of shh expression. Dev Biol 211:53-63.

734 Jho EH, Zhang T, Domon C, Joo CK, Freund JN, Costantini F (2002) Wnt/beta-catenin/Tcf signaling
735 induces the transcription of Axin2, a negative regulator of the signaling pathway. Mol Cell Biol
736 22:1172-1183.

737 Klimova L, Kozmik Z (2014) Stage-dependent requirement of neuroretinal Pax6 for lens and retina
738 development. Development 141:1292-1302.

739 Kumar S, Duester G (2010) Retinoic acid signaling in perioptic mesenchyme represses Wnt signaling
740 via induction of Pitx2 and Dkk2. Dev Biol 340:67-74.

741 Lamb TD, Collin SP, Pugh EN, Jr. (2007) Evolution of the vertebrate eye: opsins, photoreceptors,
742 retina and eye cup. Nat Rev Neurosci 8:960-976.

743 Lee JE, Wu SF, Goering LM, Dorsky RI (2006) Canonical Wnt signaling through Lef1 is required for
744 hypothalamic neurogenesis. Development 133:4451-4461.

745 Lieven O, Ruther U (2011) The Dkk1 dose is critical for eye development. Dev Biol 355:124-137.

746 Liu C, Nathans J (2008) An essential role for frizzled 5 in mammalian ocular development.
747 Development 135:3567-3576.

748 Liu C, Bakeri H, Li T, Swaroop A (2012) Regulation of retinal progenitor expansion by Frizzled
749 receptors: implications for microphthalmia and retinal coloboma. Hum Mol Genet 21:1848-1860.

750 Liu C, Widen SA, Williamson KA, Ratnapriya R, Gerth-Kahlert C, Rainger J, Alur RP, Strachan E,
751 Manjunath SH, Balakrishnan A, Floyd JA, Consortium UK, Li T, Waskiewicz A, Brooks BP, Lehmann OJ,
752 FitzPatrick DR, Swaroop A (2016) A secreted WNT-ligand-binding domain of FZD5 generated by a
753 frameshift mutation causes autosomal dominant coloboma. Hum Mol Genet 25:1382-1391.

754 Liu H, Mohamed O, Dufort D, Wallace VA (2003) Characterization of Wnt signaling components and
755 activation of the Wnt canonical pathway in the murine retina. Dev Dyn 227:323-334.

756 Loh KM, van Amerongen R, Nusse R (2016) Generating Cellular Diversity and Spatial Form: Wnt
757 Signaling and the Evolution of Multicellular Animals. Dev Cell 38:643-655.

758 Lohnes D, Mark M, Mendelsohn C, Dolle P, Dierich A, Gorry P, Gansmuller A, Chambon P (1994)
759 Function of the retinoic acid receptors (RARs) during development (I). Craniofacial and skeletal
760 abnormalities in RAR double mutants. Development 120:2723-2748.

761 Lupo G, Gestri G, O'Brien M, Denton RM, Chandraratna RA, Ley SV, Harris WA, Wilson SW (2011)
762 Retinoic acid receptor signaling regulates choroid fissure closure through independent mechanisms
763 in the ventral optic cup and periocular mesenchyme. Proc Natl Acad Sci U S A 108:8698-8703.

764 Mann B, Gelos M, Siedow A, Hanski ML, Gratchev A, Ilyas M, Bodmer WF, Moyer MP, Riecken EO,
765 Buhr HJ, Hanski C (1999) Target genes of beta-catenin-T cell-factor/lymphoid-enhancer-factor
766 signaling in human colorectal carcinomas. Proc Natl Acad Sci U S A 96:1603-1608.

767 Martynoga B, Morrison H, Price DJ, Mason JO (2005) Foxg1 is required for specification of ventral
768 telencephalon and region-specific regulation of dorsal telencephalic precursor proliferation and
769 apoptosis. Dev Biol 283:113-127.

770 McCloy RA, Rogers S, Caldon CE, Lorca T, Castro A, Burgess A (2014) Partial inhibition of Cdk1 in G 2
771 phase overrides the SAC and decouples mitotic events. Cell Cycle 13:1400-1412.

772 Memberg SP, Hall AK (1995) Dividing neuron precursors express neuron-specific tubulin. J Neurobiol
773 27:26-43.

774 Montcouquiol M, Sans N, Huss D, Kach J, Dickman JD, Forge A, Rachel RA, Copeland NG, Jenkins NA,
775 Bogani D, Murdoch J, Warchol ME, Wenthold RJ, Kelley MW (2006) Asymmetric localization of
776 Vangl2 and Fz3 indicate novel mechanisms for planar cell polarity in mammals. J Neurosci 26:5265-
777 5275.

778 Morcillo J, Martinez-Morales JR, Trousse F, Fermin Y, Sowden JC, Bovolenta P (2006) Proper
779 patterning of the optic fissure requires the sequential activity of BMP7 and SHH. Development
780 133:3179-3190.

781 Muzio L, Mallamaci A (2005) Foxg1 confines Cajal-Retzius neuronogenesis and hippocampal
782 morphogenesis to the dorsomedial pallium. J Neurosci 25:4435-4441.

783 Nguyen M, Arnheiter H (2000) Signaling and transcriptional regulation in early mammalian eye
784 development: a link between FGF and MITF. Development 127:3581-3591.

785 Noh H, Lee H, Park E, Park S (2016) Proper closure of the optic fissure requires ephrin A5-EphB2-JNK
786 signaling. Development 143:461-472.

787 Nornes HO, Dressler GR, Knapik EW, Deutsch U, Gruss P (1990) Spatially and temporally restricted
788 expression of Pax2 during murine neurogenesis. Development 109:797-809.

789 Ozeki H, Ogura Y, Hirabayashi Y, Shimada S (2000) Apoptosis is associated with formation and
790 persistence of the embryonic fissure. Curr Eye Res 20:367-372.

791 Picker A, Cavodeassi F, Machate A, Bernauer S, Hans S, Abe G, Kawakami K, Wilson SW, Brand M
792 (2009) Dynamic coupling of pattern formation and morphogenesis in the developing vertebrate
793 retina. PLoS Biol 7:e1000214.

794 Pratt T, Tian NM, Simpson TI, Mason JO, Price DJ (2004) The winged helix transcription factor Foxg1
795 facilitates retinal ganglion cell axon crossing of the ventral midline in the mouse. Development
796 131:3773-3784.

797 Puschel AW, Westerfield M, Dressler GR (1992) Comparative analysis of Pax-2 protein distributions
798 during neurulation in mice and zebrafish. Mech Dev 38:197-208.

799 Richardson M, Redmond D, Watson CJ, Mason JO (1999) Mouse Wnt8B is expressed in the
800 developing forebrain and maps to chromosome 19. Mamm Genome 10:923-925.

801 Roy A, de Melo J, Chaturvedi D, Thein T, Cabrera-Socorro A, Houart C, Meyer G, Blackshaw S, Tole S
802 (2013) LHX2 is necessary for the maintenance of optic identity and for the progression of optic
803 morphogenesis. J Neurosci 33:6877-6884.

804 Sargeant TJ, Day DJ, Miller JH, Steel RW (2008) Acute in utero morphine exposure slows G2/M phase
805 transition in radial glial and basal progenitor cells in the dorsal telencephalon of the E15.5 embryonic
806 mouse. The European journal of neuroscience 28:1060-1067.

807 Schimmenti LA (2011) Renal coloboma syndrome. Eur J Hum Genet 19:1207-1212.

808 Schimmenti LA, Pierpont ME, Carpenter BL, Kashtan CE, Johnson MR, Dobyns WB (1995) Autosomal
809 dominant optic nerve colobomas, vesicoureteral reflux, and renal anomalies. Am J Med Genet
810 59:204-208.

811 Schwarz M, Cecconi F, Bernier G, Andrejewski N, Kammandel B, Wagner M, Gruss P (2000) Spatial
812 specification of mammalian eye territories by reciprocal transcriptional repression of Pax2 and Pax6.
813 Development 127:4325-4334.

814 See AW, Clagett-Dame M (2009) The temporal requirement for vitamin A in the developing eye:
815 mechanism of action in optic fissure closure and new roles for the vitamin in regulating cell
816 proliferation and adhesion in the embryonic retina. Dev Biol 325:94-105.

817 Shaulian E, Karin M (2002) AP-1 as a regulator of cell life and death. Nat Cell Biol 4:E131-136.

818 Shiver BD, Borders BE (1996) Sampling techniques for forest resource inventory.

819 Takahashi H, Shintani T, Sakuta H, Noda M (2003) CBF1 controls the retinotectal topographical map
820 along the anteroposterior axis through multiple mechanisms. Development 130:5203-5215.

821 Tang K, Xie X, Park JI, Jamrich M, Tsai S, Tsai MJ (2010) COUP-TFs regulate eye development by
822 controlling factors essential for optic vesicle morphogenesis. Development 137:725-734.

823 Tian NM, Pratt T, Price DJ (2008) Foxg1 regulates retinal axon pathfinding by repressing an ipsilateral
824 program in nasal retina and by causing optic chiasm cells to exert a net axonal growth-promoting
825 activity. Development 135:4081-4089.

826 Tissir F, Bar I, Jossin Y, De Backer O, Goffinet AM (2005) Protocadherin Celsr3 is crucial in axonal tract
827 development. Nat Neurosci 8:451-457.

828 Torres M, Gomez-Pardo E, Gruss P (1996) Pax2 contributes to inner ear patterning and optic nerve
829 trajectory. Development 122:3381-3391.

830 Walther C, Gruss P (1991) Pax-6, a murine paired box gene, is expressed in the developing CNS.
831 Development 113:1435-1449.

832 Wen W, Pillai-Kastoori L, Wilson SG, Morris AC (2015) Sox4 regulates choroid fissure closure by
833 limiting Hedgehog signaling during ocular morphogenesis. Dev Biol 399:139-153.

834 Williamson KA, FitzPatrick DR (2014) The genetic architecture of microphthalmia, anophthalmia and
835 coloboma. Eur J Med Genet 57:369-380.

836 Wisdom R, Johnson RS, Moore C (1999) c-Jun regulates cell cycle progression and apoptosis by
837 distinct mechanisms. EMBO J 18:188-197.

838 Xuan S, Baptista CA, Balas G, Tao W, Soares VC, Lai E (1995) Winged helix transcription factor BF-1 is
839 essential for the development of the cerebral hemispheres. Neuron 14:1141-1152.

840 Yuasa J, Hirano S, Yamagata M, Noda M (1996) Visual projection map specified by topographic
841 expression of transcription factors in the retina. Nature 382:632-635.

842 Zhou CJ, Molotkov A, Song L, Li Y, Pleasure DE, Pleasure SJ, Wang YZ (2008) Ocular coloboma and
843 dorsoventral neuroretinal patterning defects in Lrp6 mutant eyes. Dev Dyn 237:3681-3689.

844 **Figure Legends**

845 **Figure 1: *Foxg1* mRNA expression in the developing optic neuroepithelium.** In E10.5 horizontal
846 sections along the ventral-to-dorsal axis, *Foxg1* is expressed in the nasal retina (r), retinal pigment
847 epithelium (RPE) and optic stalk (OS) (A-D; a-d). Strong *Foxg1* expression is detected in the
848 telencephalon (Tel). The arrow in (a) demarcates the forming optic fissure (OF). In this and all
849 subsequent images N-T designates the nasal-temporal axis marked with dashed lines in b-d; pRPE,
850 presumptive RPE. Scale bars: A-D = 100 μm; a-d = 50 μm; inset in A = 200 μm.

851 **Figure 2: Expression of Wnt molecules in the developing telencephalon and optic**
852 **neuroepithelium.** E12.5 wild type horizontal sections depicting expression of *Wnt8b* (A), *Wnt7b* (C),
853 *Wnt2b* (E), *Wnt5a* (G) and *Wnt3a* (I) in the dorsomedial telencephalon (dmTel) and cortical hem (ch).
854 *Wnt8b* is detected in the optic stalk (OS) (B, arrowhead in b) and the hypothalamic optic recess (or)
855 (arrow in b). *Wnt7b* is expressed in the lens (D, d). *Wnt7b* is also expressed strongly in the
856 diencephalic preoptic area (POA) and anterior hypothalamus (AH) (D). *Wnt2b* is expressed in the
857 ciliary margin (CM) and peripheral retinal pigment epithelium (RPE) (F, f). *Wnt5a* is detected in the
858 eyelid epithelium (arrow in H) but similar to *Wnt3a* it is not detected within the optic neuroepithelium
859 (H,h,J, j). Scale bars: A,C,E,G,I = 400 μm; B,D,F,H,J = 200 μm; b,d,f,h,j = 100 μm.

860 **Figure 3: Upregulation of *Wnt8b* expression in the nasal optic stalk in the *Foxg1-/-* mutant at**
861 **E10.5.** *Wnt8b* is expressed in the dorsomedial telencephalon (Tel) (A) and in a small domain in the
862 optic stalk (OS) of controls (bracketed area in a, B, b) and is upregulated in the *Foxg1-/-* mutant
863 telencephalon (A') and in the nasal OS (arrows in a',B',b') where Foxg1 would normally be
864 expressed (β-gal staining in B,b,B',b'). Scale bars: A,A' = 200 μm; a,a',B,B' = 100 μm; b,b' = 50
865 μm.

866 **Figure 4: The *Wnt8b-/-* null mutant shows normal optic cup morphology and marker**
867 **expression.** Horizontal sections of E15.5 wild types (*Wnt8b+/+*) (A-C) and *Wnt8b-/-* mutants (A'-C')
868 do not reveal any gross differences among genotypes. Cresyl violet wild type (A) and *Wnt8b-/-*
869 mutant (A') sections reveal normal optic cup morphology. Double immunofluorescence for BrdU &
870 Tuj1 (B, B') and Vsx2 & Islet1 (C, C') show that the proliferating, outer neuroblastic layer (onbl)

(BrdU- and Vsx2-positive cells) and differentiating, inner neuroblastic layer (inbl) (Tuj1- and Islet1-positive cells) retinal layers are similar in wild types (B, C) and *Wnt8b-/-* mutants (B', C'). Scale bars: A,A', 200 μm; B,B'C,C', 200 μm.

Figure 5: Rescue of the coloboma phenotype of the *Foxg1-/-* mutant in a *Foxg1-/-;Wnt8b-/-* null background. Optic cup images of control embryos showing normal optic fissure closure (A), *Foxg1-/-;Wnt8b+/+* single mutants with a large ventral coloboma (A') and *Foxg1-/-;Wnt8b-/-* double mutants displaying rescue of the coloboma phenotype (A''). Cresyl violet stained sections of control (B), *Foxg1-/-;Wnt8b+/+* single (B') and *Foxg1-/-;Wnt8b-/-* double mutants (B'') revealing that the double mutant optic cup and optic nerve (indicated by arrow in B'') resembles that of the control (indicated by arrow in B), rather than that of the single mutant (B'). In the single mutant the OS does not form normally as indicated by the two arrows in B', resulting in abnormal formation of the optic nerve. High power images of coronal sections of control (C, D, E) and *Foxg1-/-;Wnt8b-/-* double mutants (C', D', E') in anterior (C, C'), mid-lenticular (D, D') and posterior (E, E') levels showing failure of the optic fissure to seal completely in the double mutant anterior and mid-lenticular levels (arrowheads in C' and D' respectively). Scale bars: A,A',A'', 20 μm; B,B',B'', 200 μm; C-E & C'-E', 100 μm.

Figure 6: Upregulation of *Foxd1* expression in the *Foxg1-/-* and in the *Foxg1-/-;Wnt8b-/-* double mutant nasal retina. *Foxd1* mRNA expression in horizontal E11.5 (A-A'') and E15.5 (B-B'') sections is detected in the temporal retina of controls (A, B), but is found upregulated throughout the temporal and nasal retinal domains in *Foxg1-/-;Wnt8b+/±* (A', B') and *Foxg1-/-;Wnt8b-/-* double mutants (A'', B''). Scale bars: A,A',A'', 100 μm; B,B',B'', 200 μm.

Figure 7: The shape of the nasal optic cup is compromised in *Foxg1-/-* mutants. Double immunofluorescence for Coup-TFI & Mitf in wild type (*Foxg1+/+*) ventral (A-C) and dorsal (D-F) and *Foxg1-/-* ventral (A'-C') and dorsal (D'-F') E10.5 horizontal sections. Coup-TFI is found in the ventral (A,A') and dorsal (D,D') retina (r) and in the optic stalk (OS) in both wild types (A,D) and *Foxg1-/-* mutants (A',D'). Mitf is found in the retinal pigment epithelium (RPE) in ventral and dorsal sections in both wild types (B,E) and *Foxg1-/-* mutants (B',E'). The brackets in (B) and (B') indicate

898 the presumptive RPE (pRPE) in wild types and *Foxg1-/-* mutants respectively. The asterisk in (C)
899 labels the optic fissure (OF) in wild types (C), which is not clearly visible in *Foxg1-/-* mutants
900 (question mark in C'). The double arrow in (C') indicates the abnormally enlarged distance between
901 nasal and temporal OS in the *Foxg1-/-* mutant and the arrowhead the lack of invagination of the nasal
902 optic cup. The dashed lines in (F) and (F') indicate the naso-temporal axis. Phosphorylated myosin
903 light chain 2 (pMLC2) expression in wild types (G) and *Foxg1-/-* mutants (G') is detected along the
904 RPE (indicated by small arrows in G,G') and in the hinge region (indicated by a vertical arrow in G
905 and G'). Scale bars: A-F; A'-F', 100 μm; G,G', 50 μm.

906 **Figure 8: Marker analysis of the optic neuroepithelium in control, *Foxg1-/-;Wnt8b+/+* and**
907 ***Foxg1-/-;Wnt8b-/-* E10.5 horizontal sections.** Coup-TFII (green) and Pax2 (magenta)
908 immunofluorescence in control (A,B), *Foxg1-/-;Wnt8b+/+* (A',B') and *Foxg1-/-;Wnt8b-/-* (A'',B'')
909 sections. Coup-TFII is found in the optic stalk (OS) and the presumptive retinal pigment epithelium
910 (pRPE), indicated by brackets in (A,A',A'') in ventral sections and the RPE in dorsal sections
911 (B,B',B'') in controls (A,B), single (A',B') and double mutants (A'',B''). Pax2 is found in the optic
912 stalk (A,C) and in the region of the retina (r) that surrounds the forming optic fissure in control ventral
913 sections (magenta bracketed areas in A&C). In *Foxg1-/-;Wnt8b+/+* single mutants ventral sections,
914 Pax2 is found in the OS (A',C') but expression in the retina is shifted towards the temporal domain, as
915 indicated by the magenta bracket in A' & C'. In the *Foxg1-/-;Wnt8b-/-* double mutant, Pax2 is
916 expressed in the OS (A'',C'') and throughout the retina in ventral sections (magenta bracket in A'' &
917 C''). In dorsal sections, Pax2 expression is found in the region that will give rise to the optic disc
918 (OD) (B,D,B',D',B'',D'') in all three genotypes. Dorsal Pax2 expression in the *Foxg1-/-;Wnt8b+/+*
919 mutant is shifted to the temporal retina, as with ventral sections (B',D'). Pax6 (green) and Pax2
920 (magenta) immunofluorescence in control (C,D), *Foxg1-/-;Wnt8b+/+* (C',D') and *Foxg1-/-;Wnt8b-/-*
921 (C'',D'') sections. Pax6 expression is found in the retina and RPE throughout the ventro-dorsal axis.
922 In *Foxg1-/-;Wnt8b+/+* mutants the size of the ventro-nasal Pax6+ domain is clearly enlarged (green
923 bracket in C') compared to that of controls (C) and *Foxg1-/-;Wnt8b-/-* double mutants (green bracket
924 in C''). The green brackets in A,A',A'' indicate nasal Pax2-negative expression, which corresponds to
925 Pax6-positive expression in C,C',C'', while the magenta brackets indicate the Pax2 expression

926 domain. The arrows in A',C' and A'',C'' indicate the lack of a clear constriction where the optic cup
927 invagination forms nasally in single and double mutants respectively**.** The graph (E) shows the
928 difference in the mean values of the corrected total cell fluorescence (CTCF) for Pax6 and Pax2 in the
929 nasal and temporal retinal domains along the ventro-dorsal axis. The asterisk indicates a p=0.04. An
930 ANOVA was performed to define the statistical significance of the difference of the results (F);
931 $n^{control}$= 5 eyes from 3 different embryos; $n^{Foxg1-/-;Wnt8b+/+}$= 6 eyes from 3 different embryos; $n^{Foxg1-/-;Wnt8b-/-}$= 4 eyes from 3 different embryos; Scale bars: 100 μm.

933 **Figure 9: Marker analysis of the optic neuroepithelium in control, *Foxg1-/-;Wnt8b+/±* and**
934 ***Foxg1-/-;Wnt8b-/-* E11.5 horizontal sections.** Coup-TFII (green) and Pax2 (magenta)
935 immunofluorescence in control (A-C), *Foxg1-/-;Wnt8b+/±* (A'-C') and *Foxg1-/-;Wnt8b-/-* (A''-C'')
936 sections. In ventral and middle sections, Coup-TFII is restricted in the retinal pigment epithelium
937 (RPE) (A-A'', B-B''), while in dorsal sections it is expanded at the tips of the peripheral retina
938 (arrows in C-C''). In ventral sections Pax2 is detected at the apposed edges of the optic fissure in
939 controls (A) and *Foxg1-/-;Wnt8b-/-* double mutants (A''). In *Foxg1-/-;Wnt8b+/±* mutants, Pax2
940 expression is found in the temporal but not the nasal edges of the optic fissure (A'). Pax2 is also
941 detected in the optic disc (OD) marked with arrowheads in all three different genotypes (A-A'', B-
942 B'', C- C'') and optic stalk (OS) (A-A'', D-D'', E-E''). The thin arrows in (A-A'') demarcate the
943 optic fissure (OF). Pax6 (green) and Pax2 (magenta) immunofluorescence in control (D-F), *Foxg1-/-*
944 *;Wnt8b+/±* (D'-F') and *Foxg1-/-;Wnt8b-/-* (D''-F'') sections. Pax6 expression is found in the retina
945 (r) and RPE throughout the ventro-dorsal axis. Pax6 staining reveals that the size of nasal and
946 temporal retina is similar in controls (D-F) and *Foxg1-/-;Wnt8b-/-* double mutants (D''-F''). In
947 *Foxg1-/-;Wnt8b+/±* mutants the size of the nasal retina is clearly enlarged compared to that of the
948 temporal retina (compare size of bracketed areas in D'). The asterisk in (F') marks the presence of
949 abnormal ciliary margin tissue in the *Foxg1-/-;Wnt8b+/±* mutant, as previously described (Fotaki et
950 al., 2013). Scale bars: 100 μm.

951 **Figure 10: Quantitation of Pax6 and Pax2 expression in E11.5 retinal sections.** An ANOVA was
952 performed to define the statistical significance of the difference in the mean values of the corrected

total cell fluorescence (CTCF) for Pax6 (A) and Pax2 (B) in the nasal and temporal retinal domains along the ventro-dorsal axis. The graph (C) depicts these differences and the asterisks indicate the corresponding p values; n= 4 eyes from 3 different embryos for all three groups analysed.

Figure 11: Optic fissure marker expression in control (*Foxg1*+/+; *Foxg1*+/-) and *Foxg1*-/- mutant sagittal sections. At E11.5, Foxg1 (blue staining in A, B) is expressed in the anterior (A) edge in controls (*Foxg1*+/-), while Pax2 (brown staining in A, B) is detected in both the anterior and posterior (P) edges of the optic fissure (A, B). At E12.0, Pax2 immunofluorescence reveals normal anterior and posterior expression at the optic fissure edges in the wild type (*Foxg1*+/+) (C), while in the *Foxg1*-/- mutant the anterior domain of expression is lost and the posterior is maintained (C'). Similarly, *Vax1* mRNA wild type anterior expression (D, E) is compromised in the *Foxg1*-/- mutant (D', E'), while posterior expression is intact (D, D', E, E'). *Bmp7* mRNA expression is intact in both the anterior and posterior edges of the optic fissure in the *Foxg1*-/- mutant (F', G') similar to the wild type (F, G). A, D, D', F, F' are more proximal sections to B, E, E',G, G' respectively. Scale bars: A,B, 100 μm; C,C', 100 μm; D-G & D'-G', 100 μm.

Figure 12: Pax2 expression in the anterior and posterior tips of the optic fissure. Pax2 expression in E11.5 sagittal control (A), *Foxg1*-/-;*Wnt8b*+/± mutant (A') and *Foxg1*-/-;*Wnt8b*-/- double mutant (A'') sections showing that the normal Pax2 expression in the anterior (A) and posterior (P) edges of the control optic fissure (A) is only found posteriorly in the *Foxg1*-/-;*Wnt8b*+/± mutant (A') but is rescued in the *Foxg1*-/-;*Wnt8b*-/- double mutant (A''). ANOVA analysis revealed that the Pax2-positive cells within a 0.01 mm^2 area at the edges of the nasal retina is significantly reduced ($p<0.0001$) in the *Foxg1*-/-;*Wnt8b*+/± mutants compared to that of controls and double mutants (B); $n^{control}$= 3 eyes from 3 different embryos; $n^{Foxg1-/-;Wnt8b+/\pm}$= 4 eyes from 3 different embryos; $n^{Foxg1-/-;Wnt8b-/-}$= 3 eyes from 3 different embryos. Scale bars: 100 μm.

Figure 13: Apoptotic cell density is significantly reduced in the nasal retina in the *Foxg1*-/- mutant. β-galactosidase (β-gal) staining defines the border between the nasal and temporal retinae (r) (dashed line in A, A') in *Foxg1*+/- heterozygote controls (A) and *Foxg1*-/- mutants (A'). Cleaved caspase-3 immunohistochemistry was used to detect retinal cells undergoing apoptotic cell death in

wild types (*Foxg1*+/+) (B) and *Foxg1*-/- mutants (B'). Mean apoptotic cell density values were normalized as a percentage to the wild type nasal value (100% apoptotic density) (C). Scale bars: 50 μm.

Figure 14: Partial rescue of the apoptosis phenotype of the *Foxg1*-/- mutant in the *Foxg1*-/-;*Wnt8b*-/- double mutant. Cleaved caspase-3 immunohistochemistry labels retinal cells undergoing apoptotic cell death in control (A), *Foxg1*-/-;*Wnt8b*+/± (A') and *Foxg1*-/-;*Wnt8b*-/- (A'') E10.5 horizontal sections. The arrows is A and A'' indicate the optic fissure (OF), which starts to form in the control and *Foxg1*-/-;*Wnt8b*-/- double mutant, while the dashed-arrow in A' indicates a less-clear formation of the OF in *Foxg1*-/-;*Wnt8b*+/+single mutants. Mean apoptotic cell density values were normalized as a percentage to the control nasal value (100% apoptotic density) (B). Scale bars: 50 μm.

Figure 15: Optic cup and stalk Wnt-signalling target gene analysis in controls and *Foxg1*-/- mutants at E12.5. c-Jun protein expression is upregulated in the *Foxg1*-/- optic cup (A') compared to expression in controls (A). No differences in *Fzd3* (B,B'), *Celsr3* (C,C') or *Vangl2* (D,D') mRNA expression are observed between *Foxg1*-/- mutants and controls. *Axin2* expression is upregulated in the nasal component of the optic stalk in *Foxg1*-/- mutants (arrowheads in E') compared to controls (arrow in E) and mirrors upregulated expression of *Wnt8b* in the same region (compare E to F & E' to F'). Scale bars: A,A', 100 μm; B-E, B'-E', 200 μm; F,F', 100μm.

Figure 16: Schematic summary of main findings and proposed Foxg1 regulatory network in the developing eye. In wild types (A) Foxg1 is normally expressed in the nasal optic cup (OC) and optic stalk (OS), *Wnt8b* is expressed in the nasal and temporal OS and Pax2 is expressed in the nasal and temporal OS and in the nasal and temporal edges of the optic fissure (OF). Apoptosis is normally observed in the nasal and temporal edges of the OF (brown dots). In *Foxg1*-/- mutants (B), loss of Foxg1 results in abnormal upregulation of *Wnt8b* nasally, increased suppression of Pax2 and decreased apoptotic cell death in the nasal edges of the fissure. In *Foxg1*-/-;*Wnt8b*-/- double mutants (C), loss of both Foxg1 and Wnt8b results in rescued Pax2 expression in the nasal edges of the OF, although Pax2 expression is stronger distally than proximally. Apoptosis is increased compared to the

Foxg1-/- mutant (B) but it is still significantly below the control values (A). (C-D) A model of possible molecular interactions showing how Foxg1 function and loss of function affects optic cup and optic fissure formation. The ---| symbol indicates repression; the -> activation. Our model cannot predict whether the molecular interactions are direct or indirect.

Table Legends:

Table 1: Antibodies used in this study

Table 2: Apoptotic cell densities in *Foxg1+/+* wild type and *Foxg1-/-* mutant nasal and temporal retinae. n= 5 eyes from 3 different embryos for each group; SE, standard error; 97.5% confidence interval (CI). Two cell densities are statistically different ($p<0.05$) when the confidence intervals (CI) do not intersect.

Table 3: Apoptotic cell densities in control, *Foxg1-/-;Wnt8b+/±* and *Foxg1-/-;Wnt8b-/-* nasal and temporal retinae. $n^{control}$= 6 eyes from 4 different embryos; $n^{Foxg1-/-;Wnt8b+/\pm}$ = 4 eyes from 2 different embryos; $n^{Foxg1-/-;Wnt8b-/-}$; 4 eyes from 3 different embryos; SE, standard error; 99.6% confidence interval (CI). Two cell densities are statistically different ($p<0.05$) when the confidence intervals (CI) do not intersect.

Table 4: PCR array results for 84 genes related to Wnt-mediated signal transduction, showing the average ΔC_t values for each experimental group, fold changes and the p-values of these changes. RNA was extracted from optic cups at E11.0. Results are the average values from three control and three mutant plates. The 12 gene names followed by an asterisk are downstream targets of the Wnt-signalling pathway. Fold changes >2 with a p value <0.05 were observed for *c-Jun*, *Wnt11*, *Wnt3* and *Wnt4*.

1028 **Table 1**

Primary Antibody	Source	Secondary Antibody	Reference
β-galactosidase RRID:AB_221539	rabbit; ThermoFisher Scientific (A11132)	Goat anti-rabbit biotylinated (Vector)	(Fotaki et al., 2011)
β-tubulin III (Tuj1) RRID:AB_477590	mouse; Sigma-Aldrich (T8660)	Donkey anti-mouse Alexa 568-IgG (H+L)	(Fotaki et al., 2006)
BrdU RRID:AB_10015219	mouse, clone B44; BD Biosciences, (347580)	Goat anti-mouse Alexa 488-IgG1	(Martynoga et al., 2005)
BrdU RRID:AB_305426	rat; Abcam (ab6326)	Donkey anti-rat Alexa-488-IgG (H+L)	(Fotaki et al., 2013)
cleaved Caspase-3 RRID:AB_2070042	rabbit; Cell Signalling (9664)	Goat anti-rabbit biotylinated (Vector)	(Noh et al., 2016)
Chx10 (Vsx2) RRID:AB_262173	sheep; Millipore (AB9014)	Donkey anti-sheep Alexa-488	(Klimova and Kozmik, 2014)
Coup-TFI RRID:AB_1964211	mouse; R&D Systems (PP-H8132-00)	Goat anti-mouse Alexa 488-IgG (H+L)	(Tang et al., 2010)
Coup-TFII RRID:AB_1964214	mouse; R&D Systems (PP-H7147-00)	Goat anti-mouse Alexa 488-IgG (H+L)	(Tang et al., 2010)
Islet-1 RRID:AB_1157901	mouse; DSHB (39.3F7)	Donkey anti-mouse Alexa 568-IgG (H+L)	(Fotaki et al., 2006)
Histone H3 (phospho S10) RRID:AB_304763	rabbit; Abcam (ab5176)	Goat anti-rabbit Alexa 488-IgG (H+L)	(Sargeant et al., 2008)
c-Jun RRID:AB_2130165	rabbit; Cell Signalling (60A8)	Donkey anti-rabbit Alexa 488-IgG (H+L)	Cell Signaling
Mitf RRID:AB_298801	mouse; Abcam (ab12039)	Goat anti-mouse Alexa 488-IgG (H+L)	Abcam review
Mitf	rabbit; Prof Arnheiter's lab	Goat anti-rabbit Alexa 568-IgG (H+L)	(Nguyen and Arnheiter, 2000)
pMLC2 RRID:AB_374325	rabbit; GeneTex (GTX22480)	Goat anti-rabbit Alexa 568-IgG (H+L)	(Eiraku et al., 2011)
Pax2	rabbit; ThermoFisher Scientific	Goat anti-rabbit Alexa 568-	(Burns et al.,

RRID:AB_2533990	(71-6000)	IgG (H+L)	2008)
Pax6 **RRID:AB_2315070**	mouse; DSHB	Goat anti-mouse Alexa 488-IgG1	(Fotaki et al., 2006)
Pax6 **RRID:AB_291612**	rabbit; Covance (PRB-278P)	Goat anti-rabbit Alexa 568-IgG (H+L)	(Cai et al., 2010)

1029

1030 **Table 2**

Region	Cell Density (× 10^3)	SE	97.5% CI
***Foxg1*+/+ nasal**	1.16	0.12	(0.89, 1.44)
***Foxg1*-/- nasal**	0.42	0.05	(0.31, 0.53)
***Foxg1*+/+ temporal**	0.98	0.42	(0.03, 1.93)
***Foxg1*-/- temporal**	1.19	0.3	(0.52, 1.86)

1031

1032 **Table 3**

Region	Cell Density (× 10^3)	SE	99.6% CI
control nasal	1.55	0.30	(0.75, 2.34)
Foxg1-/-;Wnt8b+/± **nasal**	0.27	0.11	(0.00, 0.54)
Foxg1-/-;Wnt8b-/- **nasal**	0.63	0.02	(0.57, 0.69)
control temporal	2.01	0.41	(0.92, 3.11)
Foxg1-/-;Wnt8b+/± **temporal**	1.11	0.17	(0.66, 1.57)
Foxg1-/-;Wnt8b-/- **temporal**	1.47	0.60	(0.00, 3.06)

1033

1034 **Table 4**

Gene Symbol	AVG ΔCt		Fold Change	P Value
	***Foxg1*-/-**	***Foxg1*+/+**		
Aes	3.34	3.43	1.06	0.922448
Apc	6.5	6.67	1.13	0.844910
Axin1	5.95	5.98	1.02	0.986177
*Axin2**	4.96	5.56	1.52	0.282091
Bcl9	5.93	6.26	1.25	0.789822
*Btrc**	6.09	6.11	1.01	0.955878
*Ccnd1**	3.2	2.87	0.8	0.446753
*Ccnd2**	3.46	3.22	0.84	0.561827
Csnk1a1	3.31	3.1	0.86	0.629207
Csnk2a1	4.64	4.48	0.9	0.725660
Ctbp1	4.51	4.52	1.01	0.868870
Ctnnb1	2.24	2.2	0.97	0.966749
Ctnnbip1	6.15	6.49	1.27	0.523909
Daam1	8.01	8.25	1.18	0.952898
*Dab2**	5.77	6.55	1.71	0.083046
Dixdc1	5.83	6.15	1.25	0.601836
Dkk1	7.4	7.22	0.88	0.575939
Dkk3	4.65	4.66	1.01	0.957113
Dvl1	6.78	6.88	1.07	0.677430
Dvl2	5.9	5.94	1.03	0.961346
Ep300	6.54	6.2	0.79	0.681840
Fbxw11	5.43	5.32	0.93	0.738350
Fbxw4	7.39	7.37	0.99	0.989112
Fgf4	Undetermined	Undetermined	-	-

*Fosl1**	15	14.2	0.57	0.462573
Foxn1	Undetermined	Undetermined	-	-
Frat1	9.02	9.17	1.11	0.633178
Frzb	7.61	9.07	2.74	0.175782
Fzd1	4.58	5.08	1.42	0.306249
Fzd2	5.28	5.89	1.52	0.330346
Fzd3	4.95	4.99	1.03	0.939483
Fzd4	5.92	6.28	1.29	0.565771
Fzd5	5.28	4.44	0.56	0.201944
Fzd6	7.42	7.67	1.19	0.505062
Fzd7	4.69	5.07	1.31	0.382821
Fzd8	8.89	9.24	1.27	0.165558
Fzd9	12.09	12.67	1.5	0.267910
Gsk3b	4.47	4.65	1.13	0.810280
*Jun**	4.42	5.74	2.5	0.019267
Kremen1	6.88	7.22	1.27	0.575288
Lef1	5.7	6.33	1.55	0.137805
Lrp5	5.41	5.71	1.23	0.340422
Lrp6	4.2	4.52	1.24	0.485828
Mapk8	5.23	5.45	1.16	0.485842
*Mmp7**	Undetermined	Undetermined	-	-
*Myc**	6.1	6.12	1.02	0.912680
Nfatc1	8.78	9.39	1.52	0.340969
Nkd1	4.89	5.23	1.27	0.215351
Nlk	6.17	5.74	0.75	0.284165
*Pitx2**	7.29	7.52	1.17	0.668072
Porcn	7.98	7.94	0.97	0.729696

*Ppard**	7.86	7.69	0.89	0.807290
Prickle1	7.02	7.76	1.67	0.173155
Pygo1	6.79	7.37	1.5	0.190255
Rhoa	3.12	2.82	0.81	0.581906
Rhou	7.2	7.16	0.97	0.932350
Ruvbl1	4.36	4	0.78	0.368340
Sfrp1	4.74	4.31	0.74	0.218370
Sfrp2	1.58	1.06	0.7	0.049288
Sfrp4	Undetermined	Undetermined	-	-
Sox17	11.66	11.61	0.96	0.922776
Tcf7	7.69	7.53	0.9	0.751242
Tcf7l1	6.68	6.76	1.06	0.762543
Tle1	6.6	6.7	1.07	0.725797
Vangl2	5	5.57	1.49	0.081913
Wif1	8.34	8.95	1.53	0.360760
*Wisp1**	11.52	12.38	1.82	0.415085
Wnt1	16.13	15.58	0.68	0.402762
Wnt10a	12.98	14.27	2.44	0.114037
Wnt11	9.62	11.86	4.73	0.042069
Wnt16	10.32	11.6	2.43	0.084045
Wnt2	Undetermined	Undetermined	-	-
Wnt2b	6.75	6.77	1.02	0.973415
Wnt3	13.7	14.88	2.26	0.005500
Wnt3a	13.97	14.96	1.99	0.206819
Wnt4	8.57	10.26	3.21	0.004796
Wnt5a	5.68	6.84	2.23	0.095104
Wnt5b	6.58	6.56	0.98	0.910277

Wnt6	7.84	8.8	1.95	0.065652
Wnt7a	12.37	12.01	0.78	0.438452
Wnt7b	9.21	9.17	0.97	0.870328
Wnt8a	Undetermined	Undetermined	-	-
Wnt8b	9.14	10.08	1.92	0.371946
Wnt9a	Undetermined	Undetermined	-	-

1035

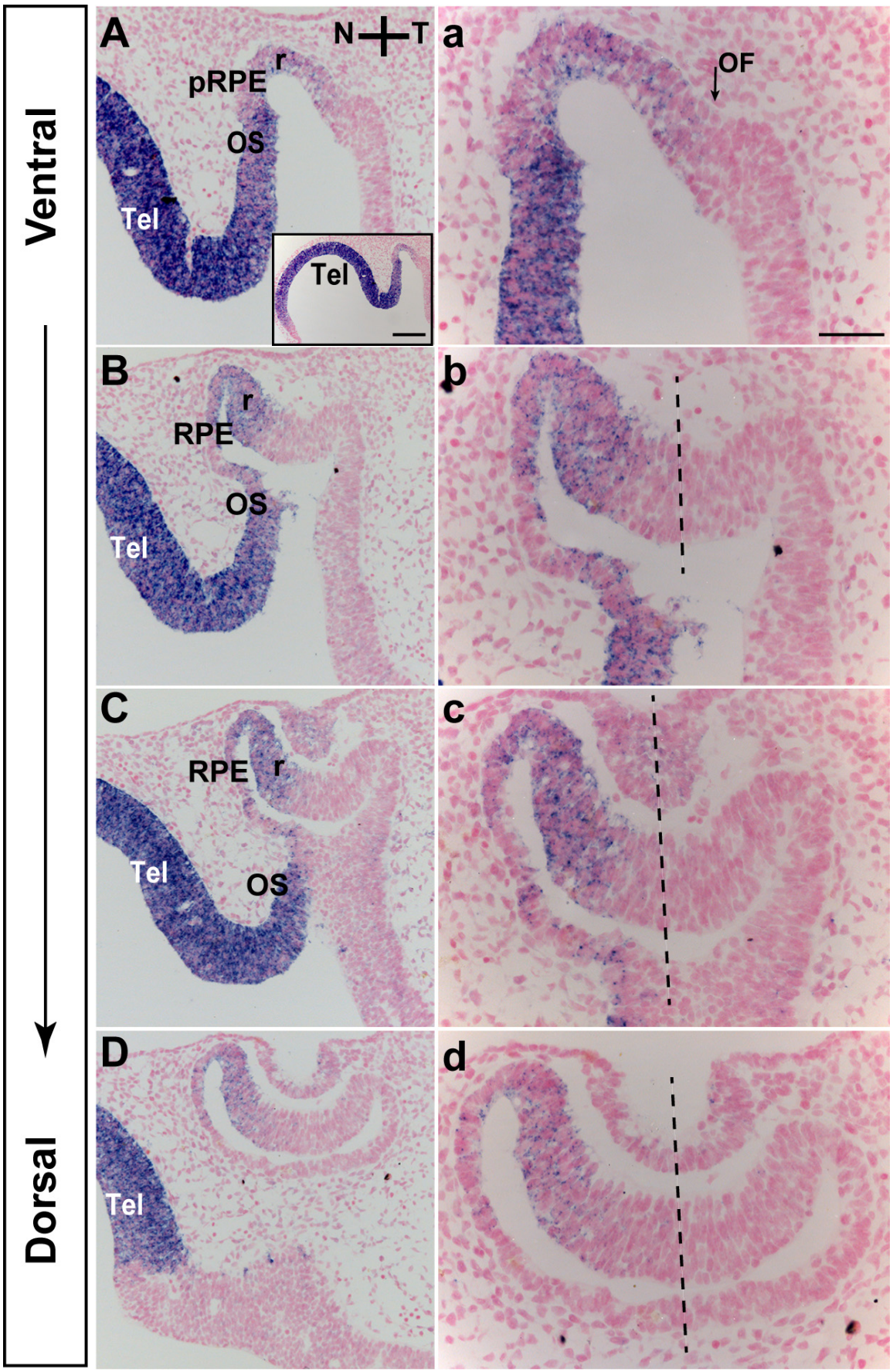

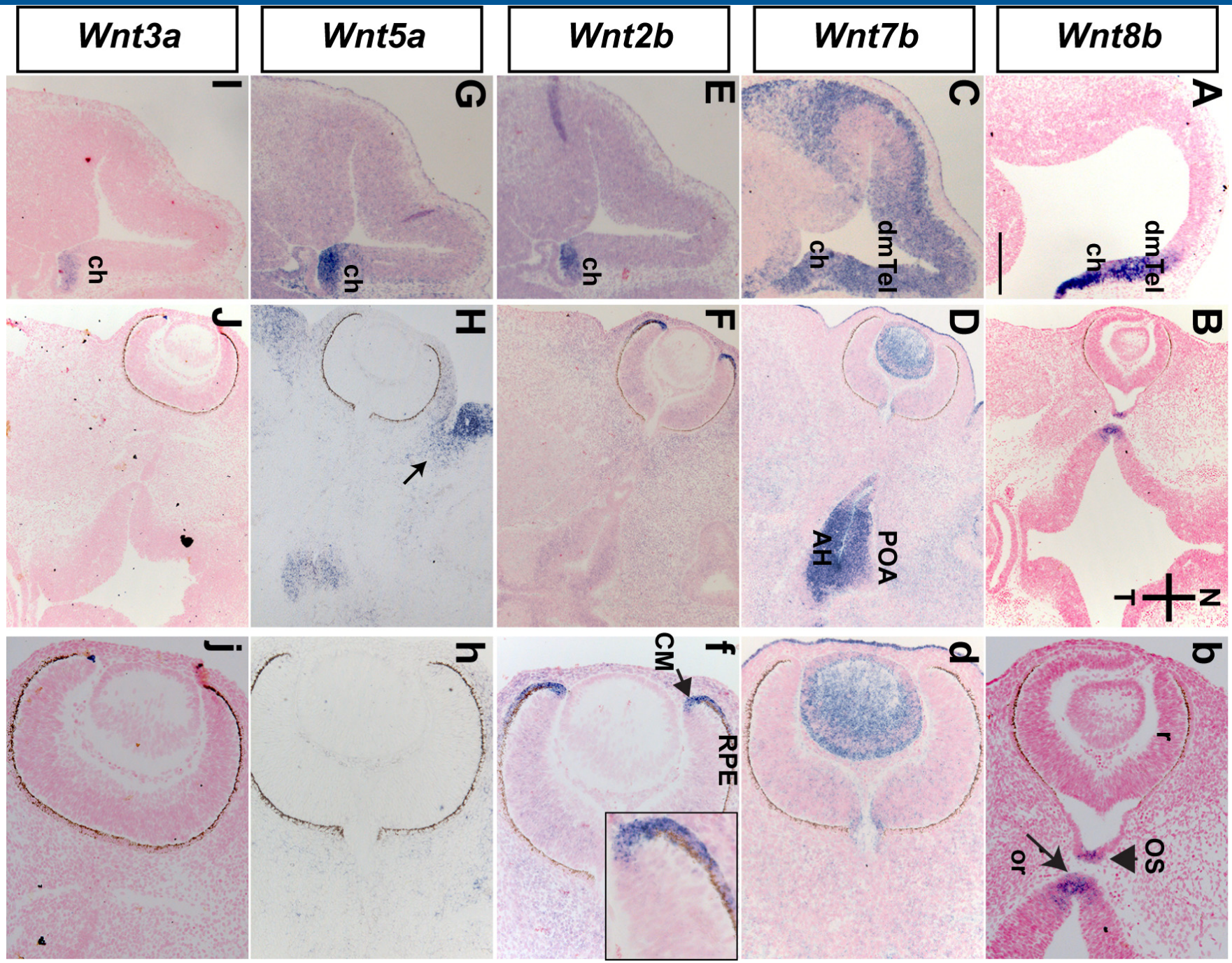

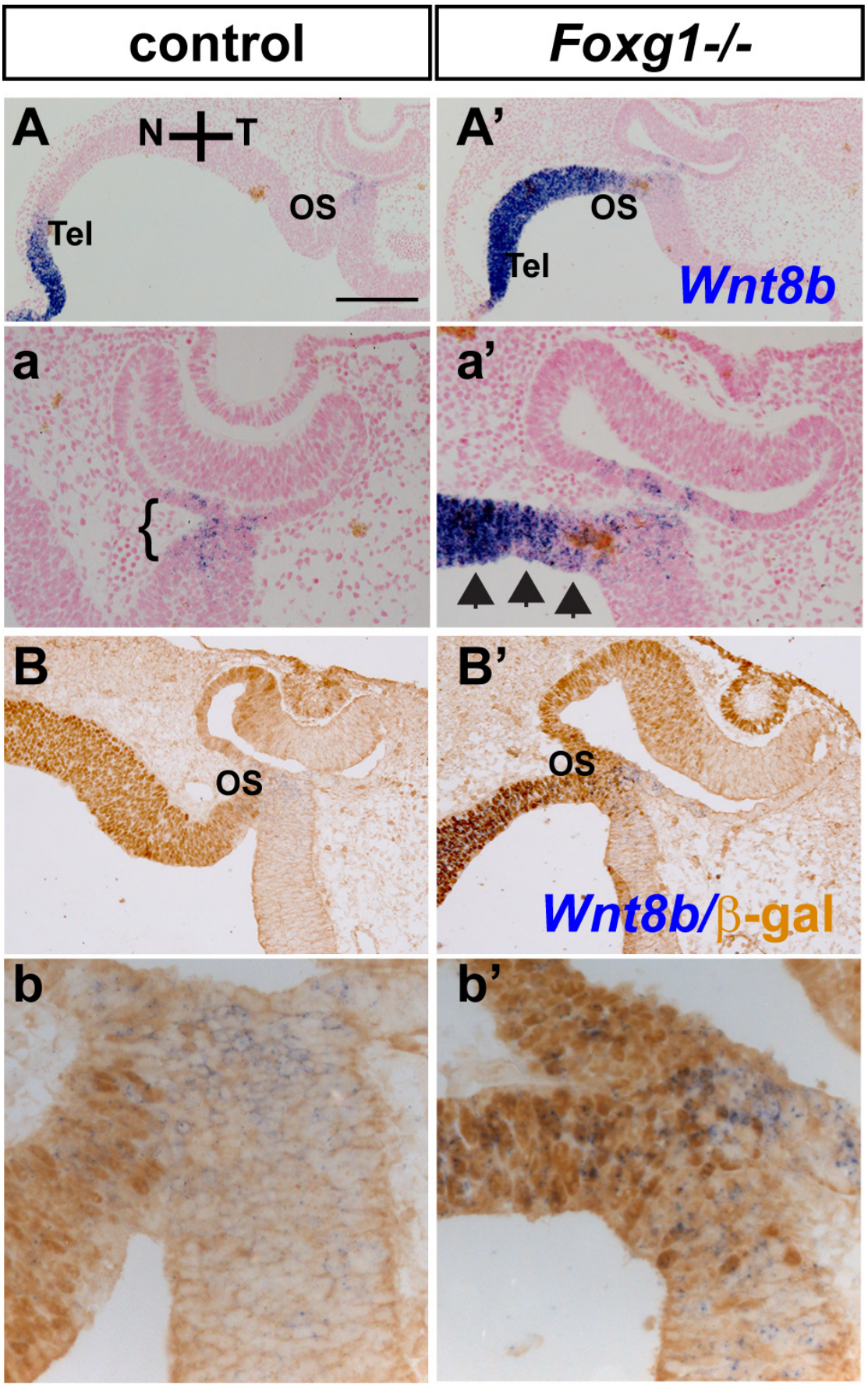

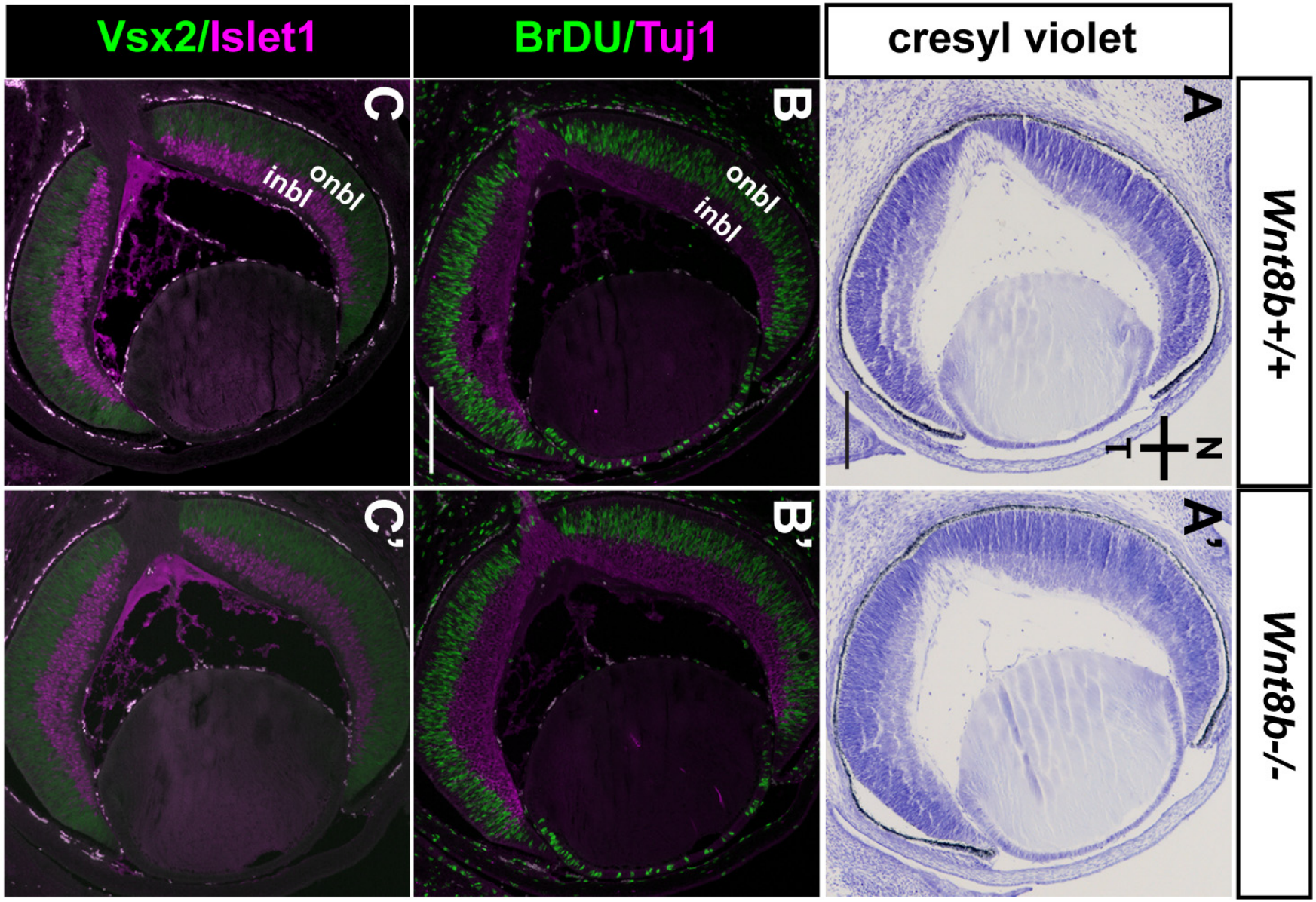
Vsx2/Islet1
BrDU/Tuj1
cresyl violet
C
B
A
onbl
inbl
onbl
inbl
T
N
C'
B'
A'
Wnt8b+/+
Wnt8b-/-

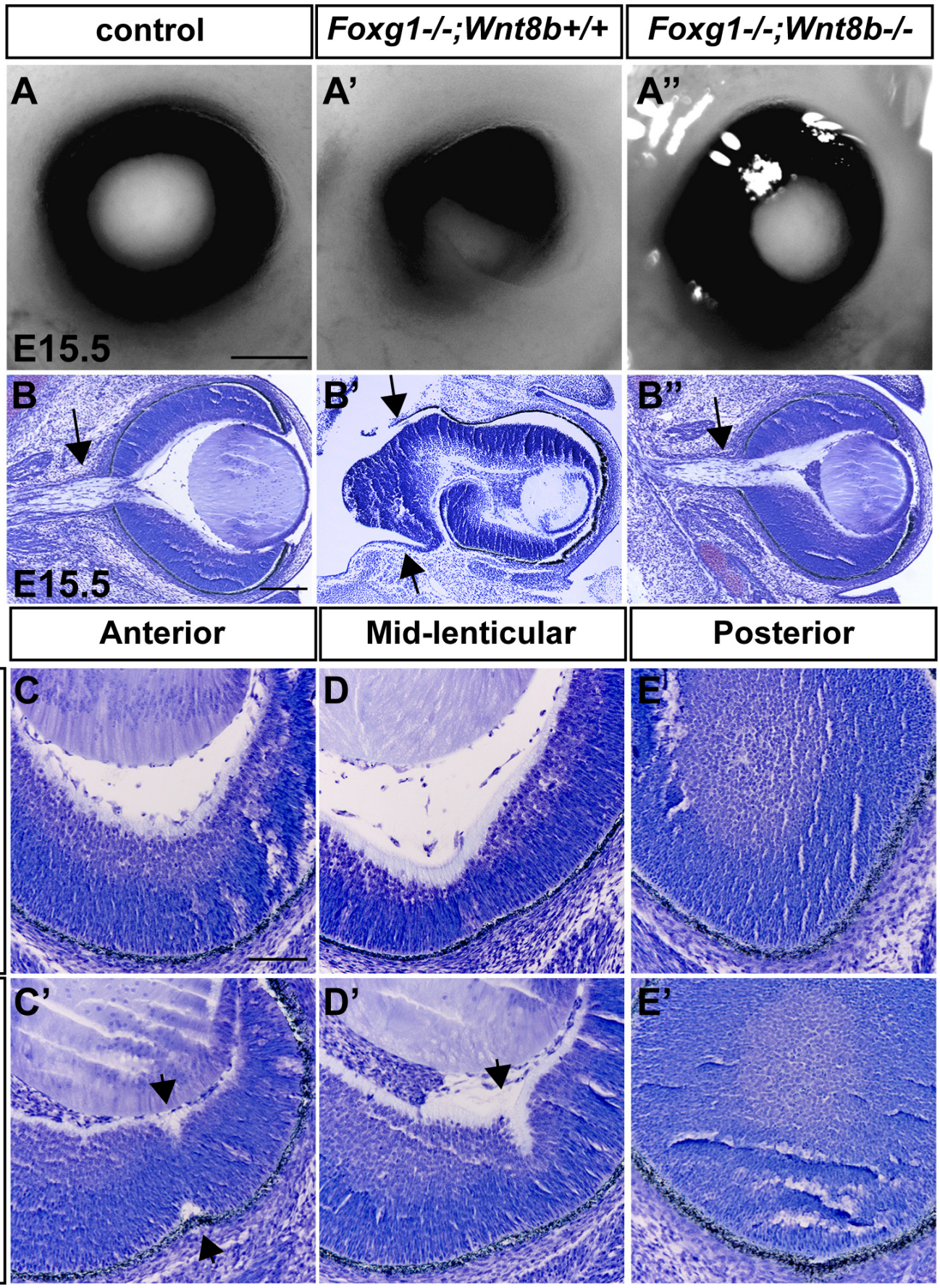

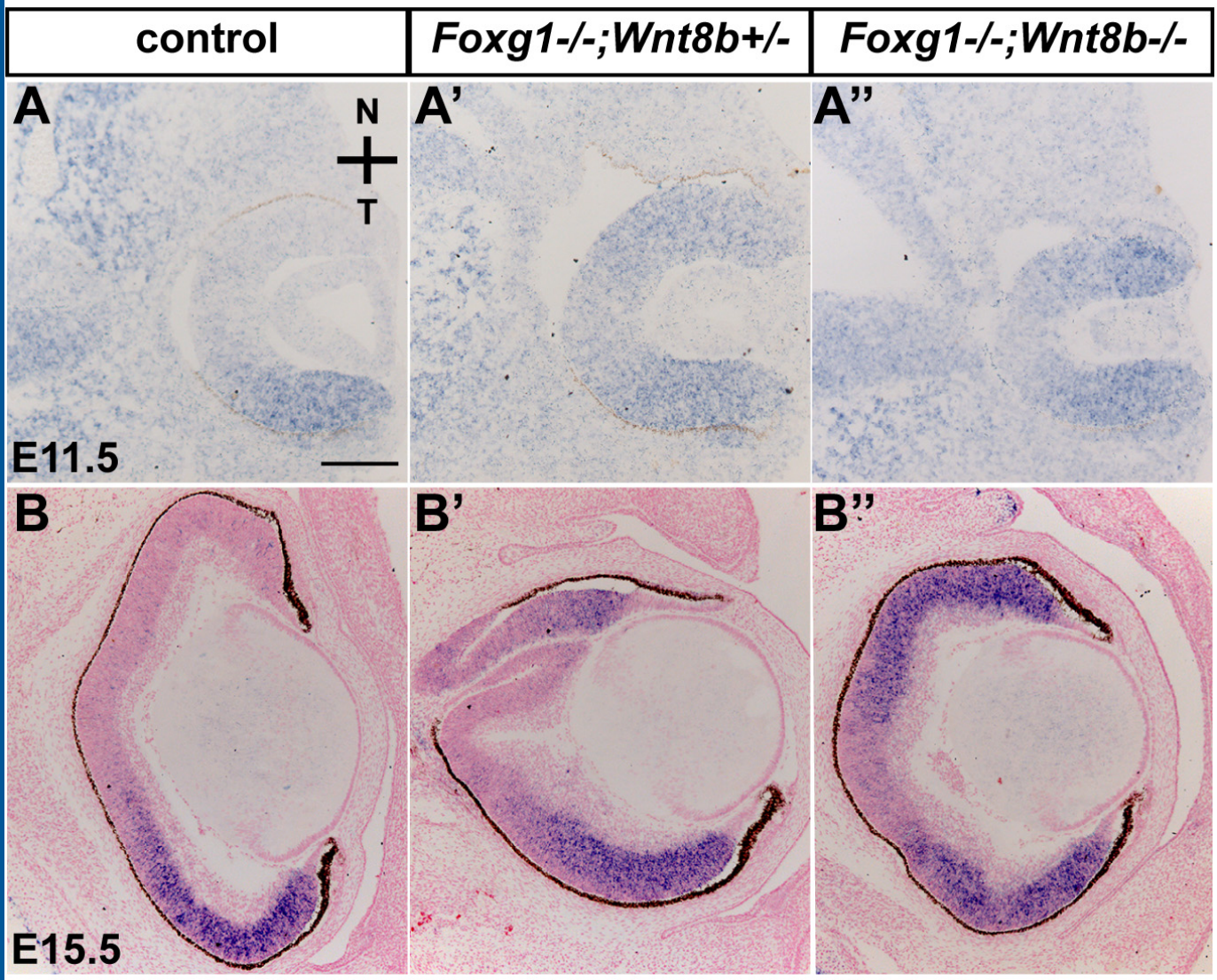

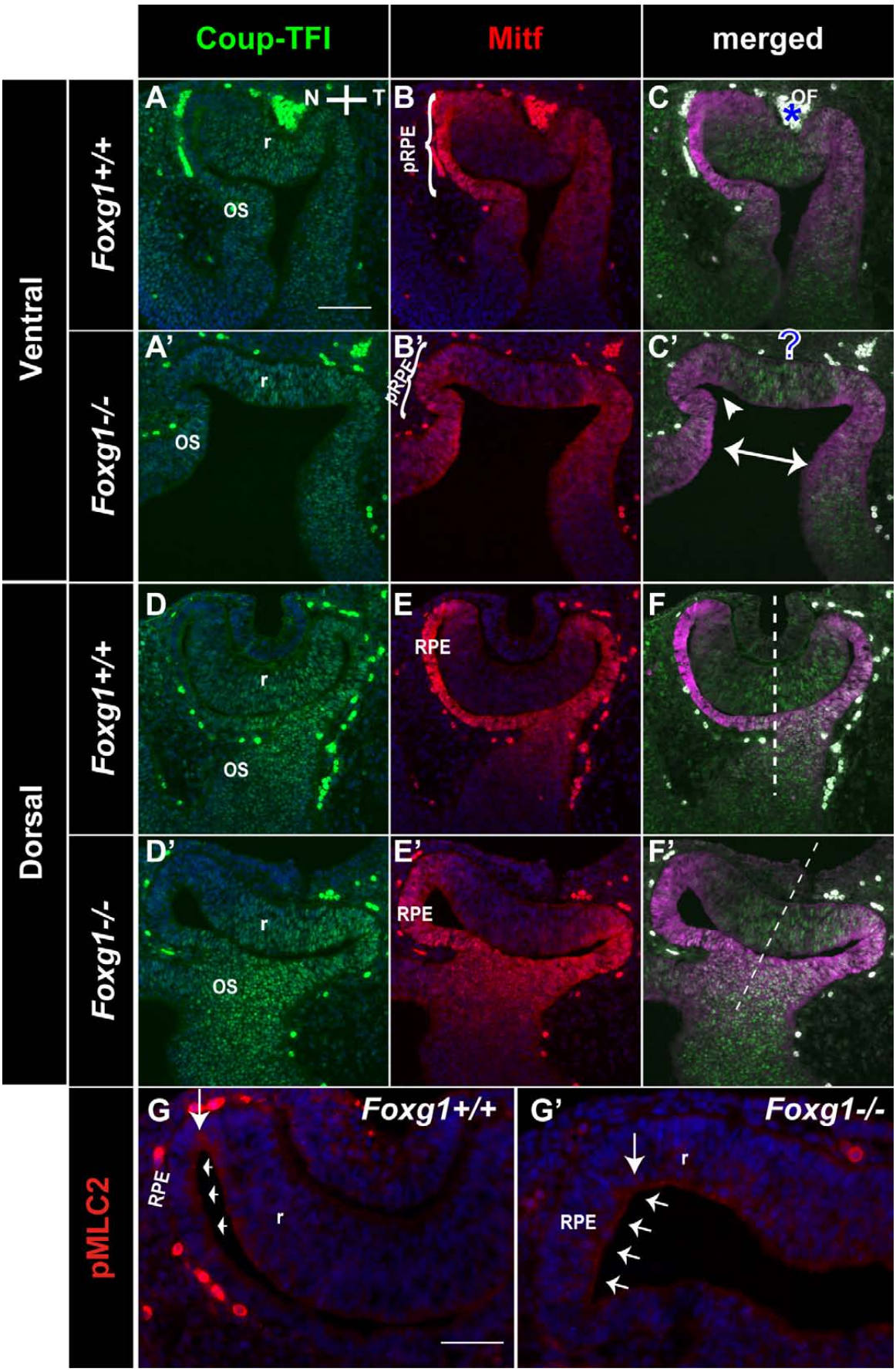

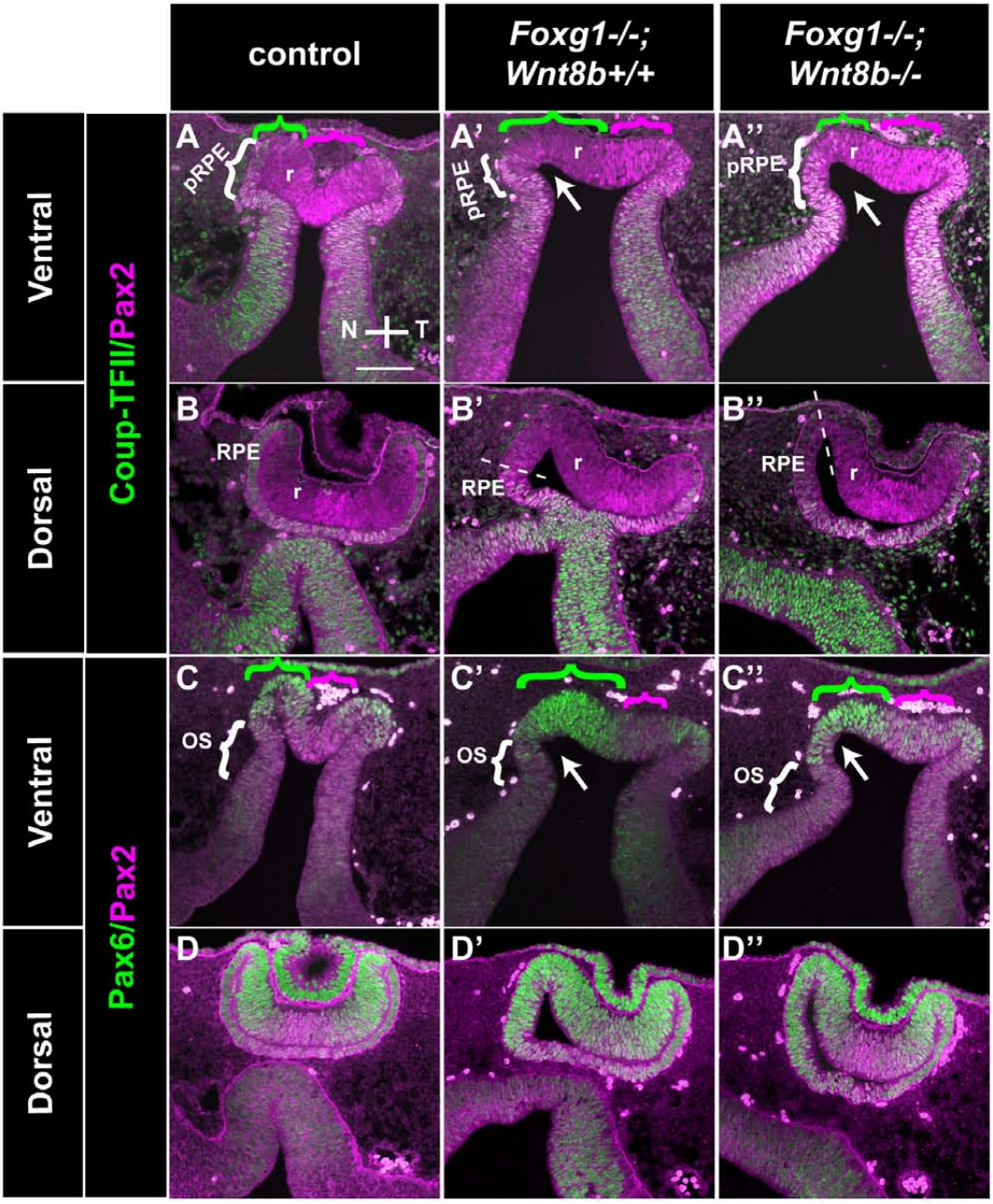

E **Corrected Total Cell Fluorescence**

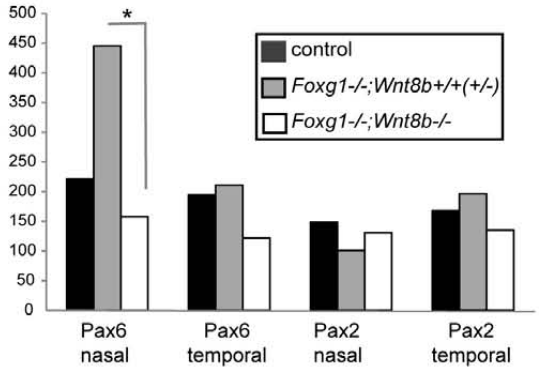

F **Nasal Pax6 CTCF**

(I) Genotype		Mean Difference (I-J)	Sig.	Confidence Lower Bound	Confidence Upper Bound
control	single mutant	-224	0.15	-510	61
	double mutant	64	1.00	-194	321
single mutant	control	224	0.15	-61	510
	double mutant	287*	0.04	13	563
double mutant	control	-64	1.00	-321	194
	single mutant	-287*	0.04	-563	-13

*. The mean difference is significant at the 0.05

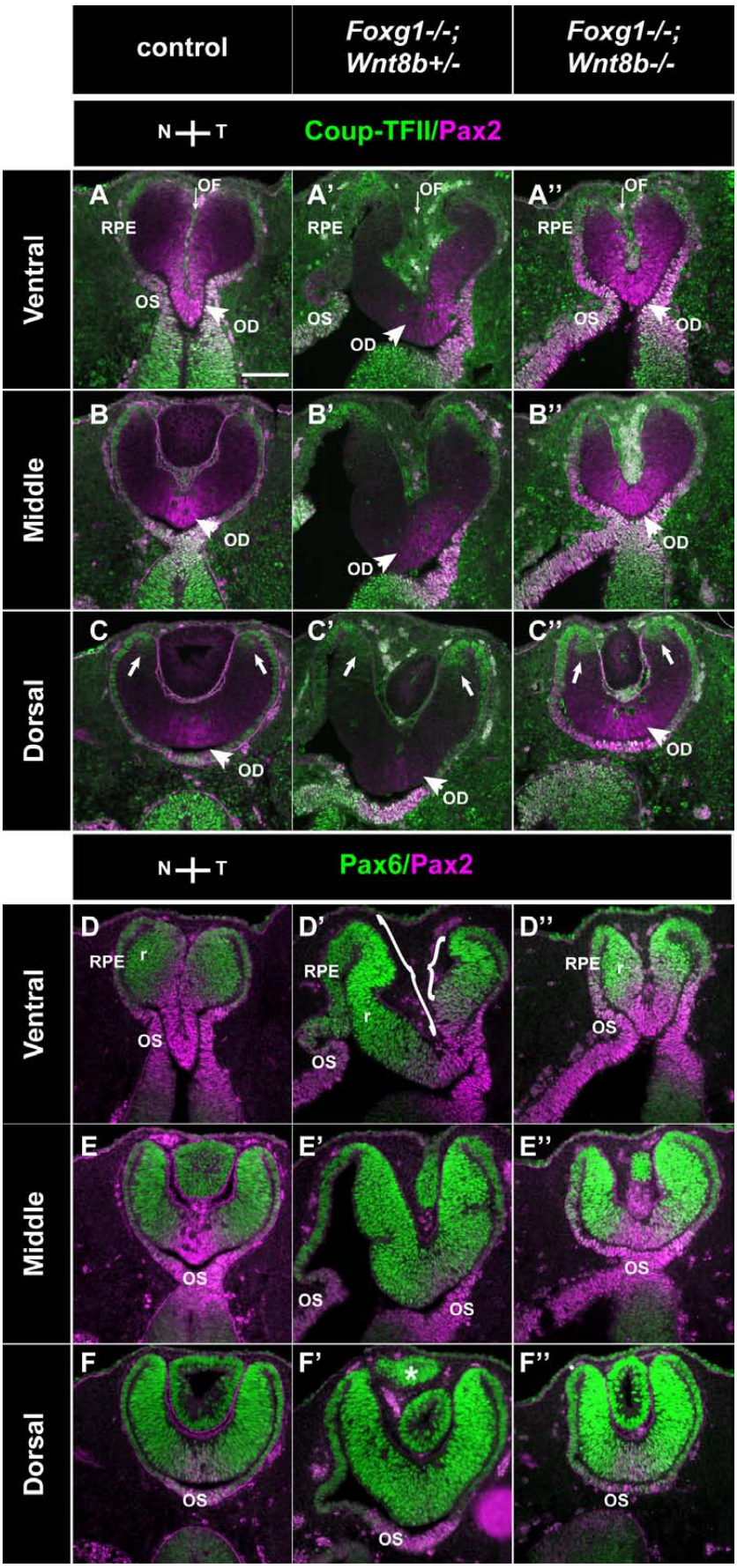

A

Nasal Pax6 CTCF

(I) Genotype		Mean Difference (I-J)	Sig.	Interval Lower Bound	Interval Upper Bound
control	single mutant	-434*	0.002	-686.0	-183.9
	double mutant	4	1.000	-260.2	269.1
single mutant	control	434*	0.002	183.9	686.0
	double mutant	439*	0.002	188.3	690.5
double mutant	control	-4	1.000	-269.1	260.2
	single mutant	-439*	0.002	-690.5	-188.3

*. The mean difference is significant at the 0.05 level.

B

Nasal Pax2 CTCF

(I) Genotype		Mean Difference (I-J)	Sig.	Interval Lower Bound	Interval Upper Bound
control	single mutant	69*	0.045	1.3	138.1
	double mutant	-94*	0.011	-166.3	-22.1
single mutant	control	-69*	0.045	-138.1	-1.3
	double mutant	-163*	0.000	-232.3	-95.5
double mutant	control	94*	0.011	22.1	166.3
	single mutant	163*	0.000	95.5	232.3

*. The mean difference is significant at the 0.05 level.

C

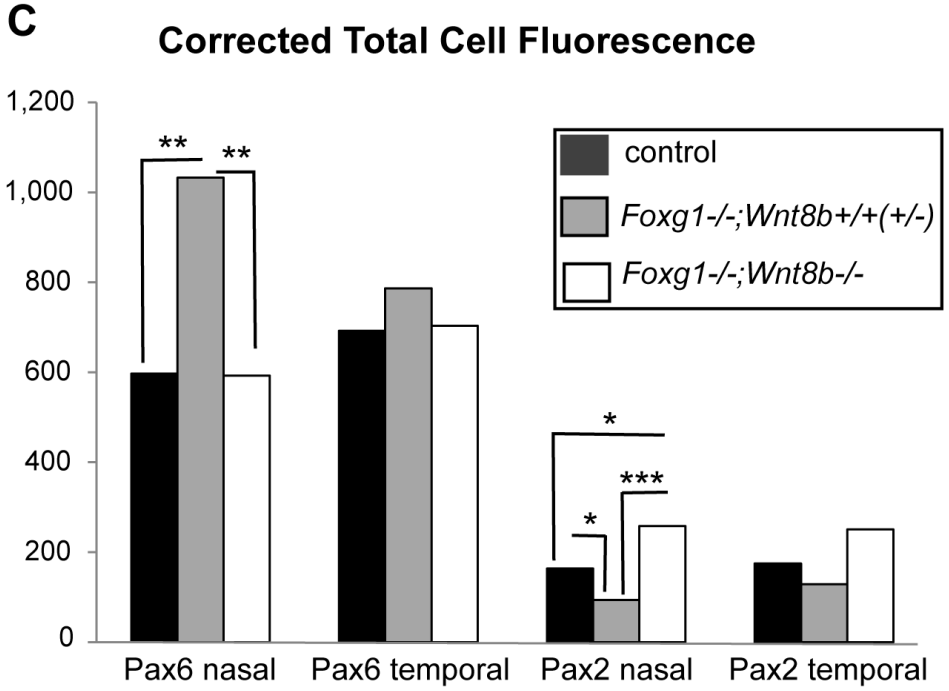

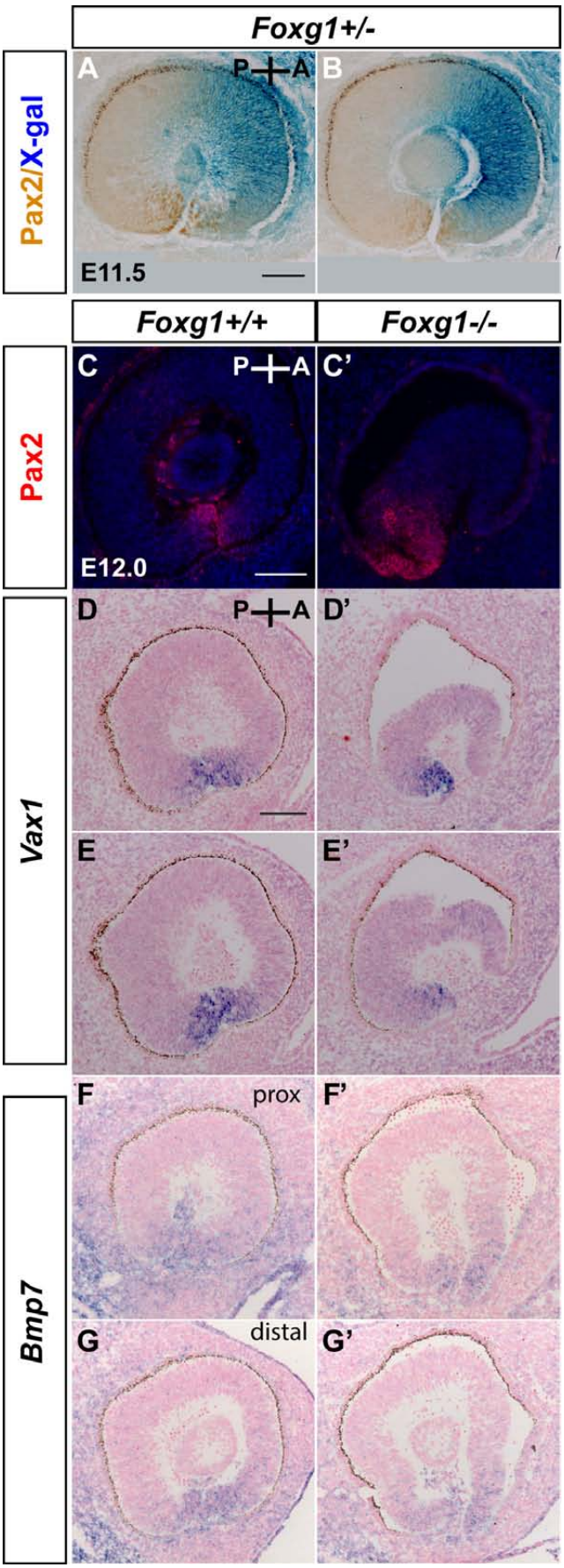

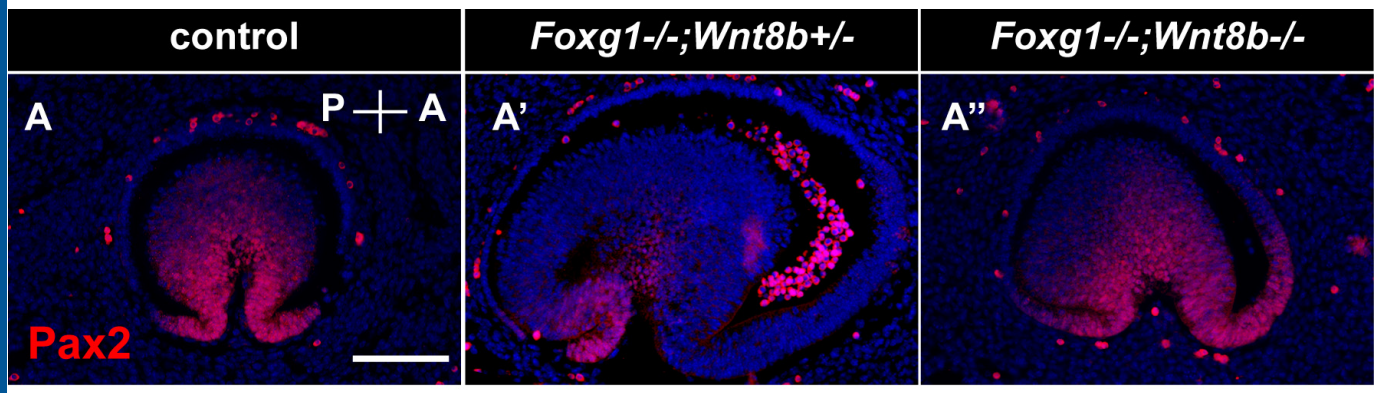

B Pax2-positive nasal cell density

(I) Genotype		Mean Difference (I-J)	Sig.	Interval Lower Bound	Interval Upper Bound
control	single mutant	15.2*	0.000	12.0	18.4
	double mutant	1.8	0.400	-1.5	5.2
single mutant	control	-15.2*	0.000	-18.4	-12.0
	double mutant	-13.4*	0.000	-16.5	-10.2
double mutant	control	-1.8	0.400	-5.2	1.5
	single mutant	13.4*	0.000	10.2	16.5

*. The mean difference is significant at the 0.05 level.